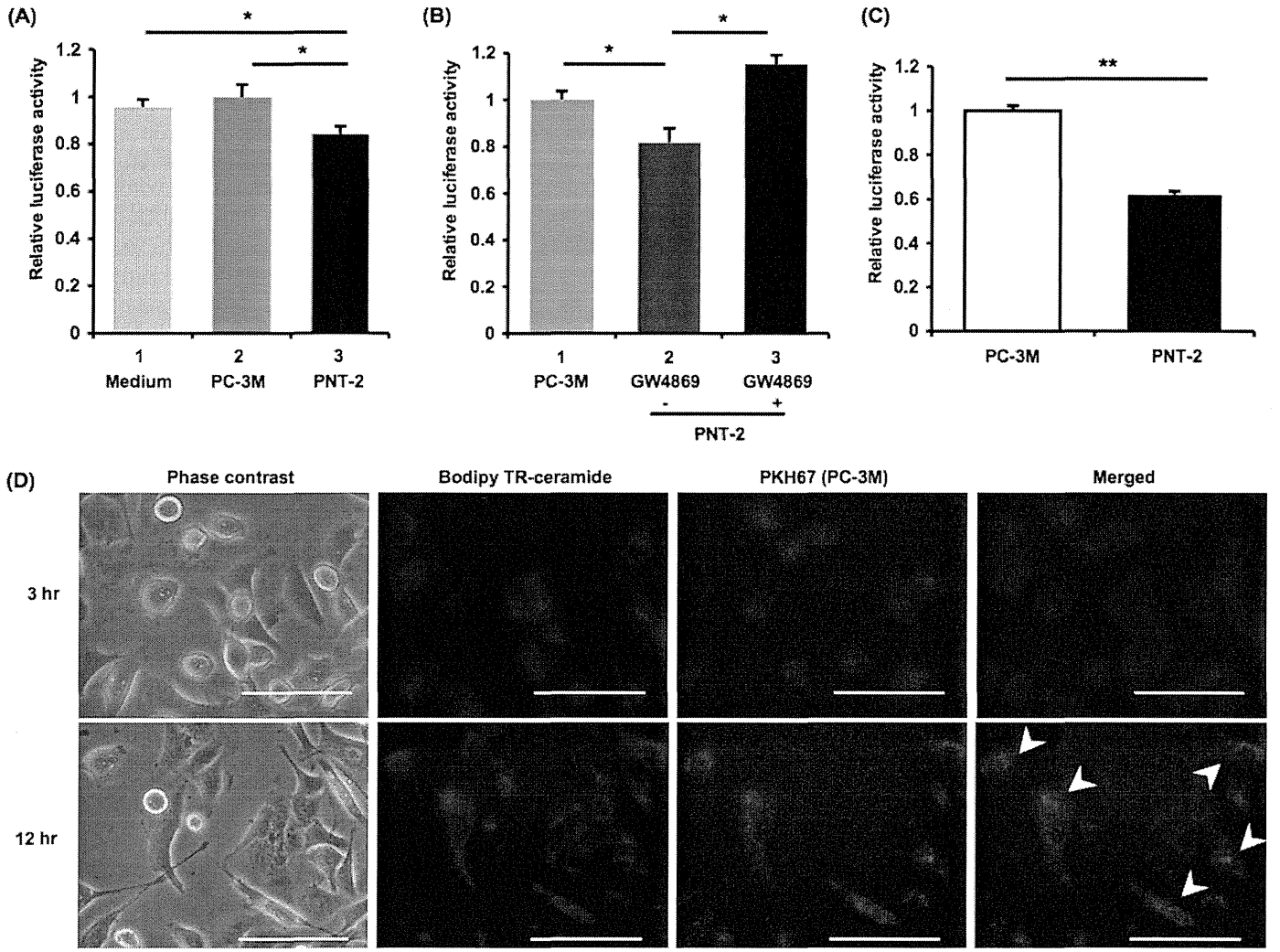

FIGURE 1. **Suppression of cancerous cell proliferation by exosome isolated from non-cancerous cells.** *A*, cell growth inhibition by a conditioned medium derived from PNT-2 cells is shown. PC-3M-luc cells were incubated for 3 days in a conditioned medium isolated from PC-3M-luc cells, PNT-2 cells, or a culture medium followed by a cell growth assay as described under "Experimental Procedures." The values on the *y* axis are depicted relative to the normalized luciferase activity of culture medium-treated cells, which is defined as 1. Each *bar* is presented as the mean S.E. ($n = 3$). *, $p < 0.05$ as compared with culture medium-treated PC-3M-luc cells; Student's *t* test. *B*, treatment with GW4869 to donor cells restored the reduced cell growth by the PNT-2-derived CM is shown. Donor PNT-2 cells were incubated in the presence or absence of 10 μM GW4869 for 2 days. The conditioned medium from PC-3M-luc cells was used as a control. The values on the *y* axis are depicted relative to the normalized luciferase activity of PC-3M-luc-conditioned medium-treated cells, which is defined as 1. Each *bar* is presented as the mean S.E. ($n = 3$). *, $p < 0.05$; Student's *t* test. *C*, cell growth inhibition by exosomes derived from PNT-2 cells is shown. PC-3M-luc cells were incubated in exosomes isolated from PNT-2 cells or PC-3M-luc cells followed by a cell growth assay, as described under "Experimental Procedures." The values on the *y* axis are depicted relative to the normalized luciferase activity of cells treated with exosomes derived from PC-3M-luc cells is defined as 1. Each *bar* is presented as the mean S.E. ($n = 3$). **, $p < 0.005$, as compared with exosomes isolated from PC-3M-luc cells; Student's *t* test. *D*, shown are fluorescent photos of BODIPY-ceramide-labeled PNT-2 and PC-3M-luc cells marked by PKH67. PNT-2 cells and PC-3M-luc cells were labeled with red fluorescent BODIPY-ceramide and green fluorescent PKH67, respectively, as described under "Experimental Procedures." After treatment of PNT-2 by BODIPY-ceramide, PKH67-labeled PC-3M-luc cells were added. After co-culturing for 3 or 12 h, images were obtained. Fluorescent photos were detected with the Eclipse TE 2000 Inverted Research Microscope, and images were produced using NIS-Elements BR software. *Arrowheads* show *yellow colored* cancer cells. The *size bar* indicates 100 μm.

of exosomes. We collected two separate aliquots of CM from PNT-2 cells incubated with or without GW4869, a specific inhibitor for neutral sphingomyelinase 2. The isolated exosomes were verified by the detection of CD63 protein, a well established exosome marker, with immunoblotting (supplemental Fig. 1*B*), and the activity of GW4869 was confirmed by the decreased amount of exosomal protein (supplemental Fig. 1*C*). The CM prepared in the presence of the GW4869 compound cancelled most tumor-suppressive activity of the non-treated PNT-2 CM (Fig. 1*B*; compare *lanes 1–3*). Furthermore, proliferation of PC-3M-luc cells was inhibited by the addition of the exosome fraction isolated from the PNT-2 CM by ultracentrifugation (Fig. 1*C*). These observations suggest that exosomal miRNAs derived from non-cancerous cells were transferred to cancerous cells, resulting in the inhibition of their proliferation.

To visualize the transfer of ceramide-containing exosome from PNT-2 to PC-3M-luc *in vitro*, a co-culture experiment was performed. Before the co-culture, 2×10^5 PNT-2 cells were incubated for 30 min with red fluorescent BODIPY-ceramide dye, which can label the exosomes inside the cells (13, 14). After washing five times with PBS, equal numbers of PC-3M-luc cells labeled by green fluorescent PKH67, a cellular membrane indicator, were added into the culture dishes. Three hours later we did not observe any PC-3M-luc cells with a yellow color (*Merged* photo in *upper panel* of Fig. 1*D*), indicating that car-

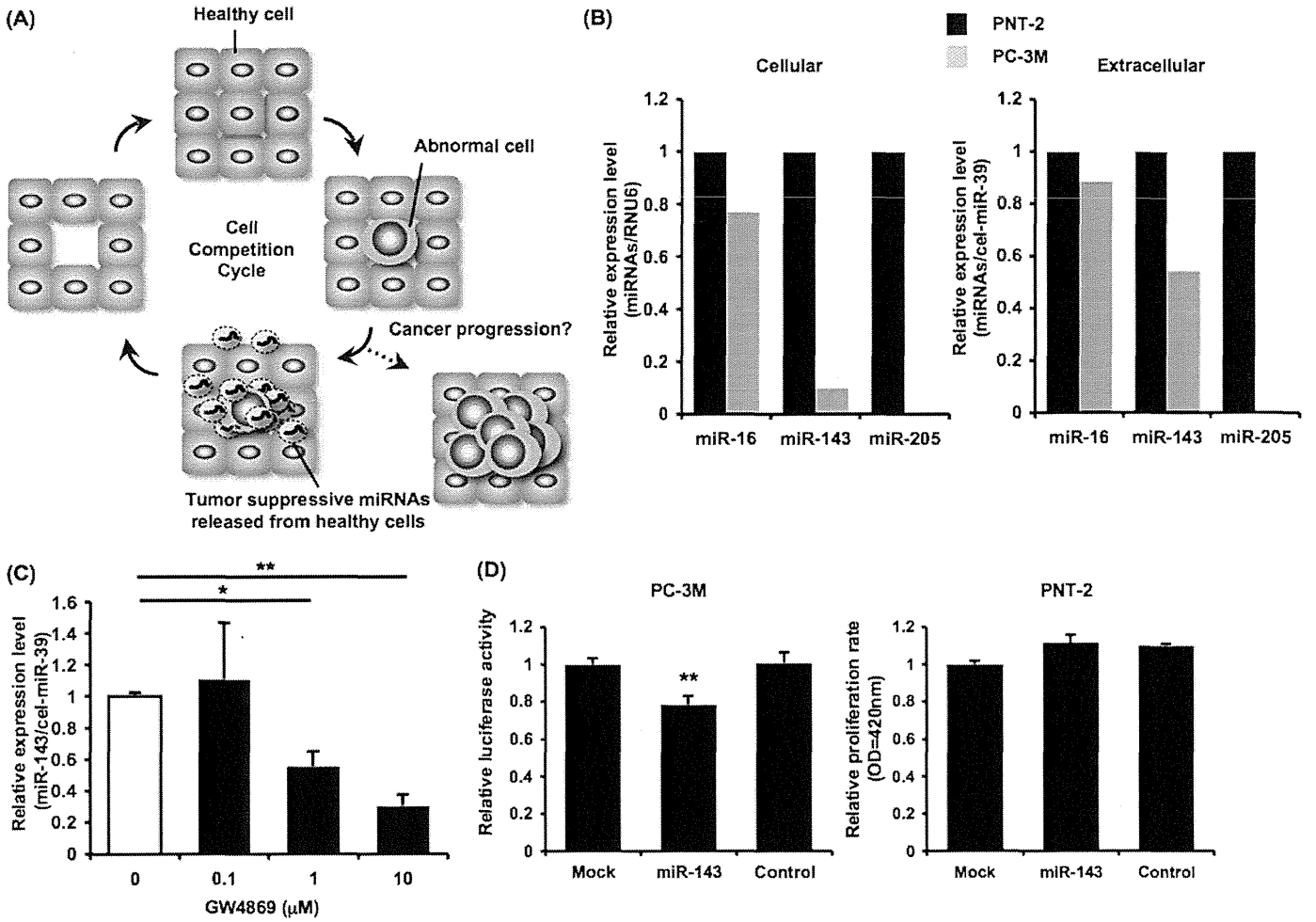

FIGURE 2. **Down-regulation of cellular and extracellular tumor-suppressive miRNAs in PC-3M-luc cells.** *A*, shown is a schematic representation of hypothetical tumor initiation process. Neighboring healthy cells (*blue*) secrete tumor-suppressive miRNAs (*light yellow*) to inhibit the proliferation of abnormal cells (gray), and this cell population returns to the initial healthy condition (a homeostatic cycle). Once the cell competitive cycle is compromised, this niche become susceptible to tumor initiation (indicated by a *dashed arrow*). *B*, comparison of cellular and extracellular miRNAs expression in PNT-2 and PC-3M-luc cells is shown. miRNA expression levels were determined by a Taq-Man QRT-PCR. The values on the *y* axis are depicted relative to the normalized expression level of PNT-2 cells, which is defined as 1. *C*, secretion of miR-143 was suppressed by the treatment with GW4869. PNT-2 cells were seeded and cultured in a 24-well plate for 48 h in the indicated concentrations of GW4869. After the incubation, the medium was subjected to QRT-PCR for miR-143. The values on the *y* axis are depicted relative to the amount of miR-143 at 0 μM GW4869, which is defined as 1. *D*, shown is cell growth inhibition by miR-143 in PC-3M-luc cells but not in PNT-2 cells. PNT-2 and PC-3M-luc cells were transfected with 10 nM miR-143 molecules (miR-143) or 10 nM negative control molecules (control) or without RNA molecules (*Mock*). The values on the *y* axis are depicted relative to the normalized luciferase activity of untreated cells (*Mock*), which is defined as 1. Each *bar* is presented as the mean S.E. ($n = 3$). *, $p < 0.05$; **, $p < 0.005$, as compared with untreated PC-3M-luc cells; Student's *t* test.

ried-over red dyes were thoroughly removed as 3 h is enough time for the dye to be incorporated directly into the cells. By contrast, after 12 h of co-culture, yellow fluorescence was observed in green-labeled PC-3M-luc cells (indicated by *arrowheads* in Merged photo in the *lower panel* of Fig. 1*D*), suggesting that ceramide-containing exosomes from PNT-2 cells were transferred to the PC-3M-luc cells. This result is corroborated by the uptake experiment using the PKH67-labeled exosomes purified from PNT-2 culture medium (supplemental Fig. 1*D*). Green fluorescence was detected in PC-3M-luc cells after 16 h of incubation, providing a direct evidence for exosome uptake by cancerous cells.

Tumor-suppressive miRNAs Down-regulated in Cancerous Cells Were Secreted from Non-cancerous Cells—We propose a hypothetical model of tumor initiation involving cell competition and anti-proliferative secretory miRNAs (Fig. 2*A*). In a cell competition cycle, as illustrated in the *bottom part* of Fig. 2*A*, growth inhibitory miRNAs are actively released from non-cancerous cells to kill abnormal cells with a partial oncogenic ability, thereby restoring them to a healthy state. Indeed, inhibitory capacity of these miRNAs appears to be limited in the setting of single treatment with the PNT-2 CM (Fig. 1*A*); however, they can potentially prevent emergence of tumor cells in a physiological condition. Because abundantly existing healthy cells continuously provide nascent overproliferative cells with tumor-suppressive miRNAs for a long period, a local concentration of secretory miRNAs can become high enough to restrain a tumor initiation. A *dashed arrow* in Fig. 2*A* indicates the way whereby the disruption of the homeostatic system leads to tumor expansion. If precancerous cells acquire resistance to anti-proliferative secretory miRNAs or normal cells cannot supply an adequate amount of miRNAs, then this defensive system will fail to maintain the healthy condition.

To test this hypothesis we checked the secretion amount of representative tumor-suppressive miRNAs by comparing PNT-2 and PC-3M-luc cells with Taq-Man QRT-PCR analysis. As shown in Fig. 2*B*, miR-16, miR-205, and miR-143, which are already reported to be dysregulated in prostate cancer (10, 15, 16), were down-regulated in PC-3M-luc cells at a cellular and extracellular level. The GW4869 inhibitor suppressed the secretion of miR-143 from PNT-2 cells in a dose-dependent manner (Fig. 2*C*), whereas its cellular level was not altered (supplemental Fig. 2*A*). Additionally, the application of small interfering RNAs specific for human neutral sphingomyelinase 2 gene knocked down its mRNAs, resulting in profound decrease in miR-143 secretion (supplemental Fig. 2, *B* and *C*). On the contrary, the expression of miR-143 in the cells was not changed after the transfection of neutral sphingomyelinase 2 siRNA (supplemental Fig. 2*D*). Taken with the result of Fig. 1*B*, these results suggest that the secreted tumor-suppressive miRNAs are implicated in the process of growth inhibition by PNT-2 CM.

For a global understanding of the expression change of non-cancerous and cancerous cells, we performed an miRNA microarray analysis against cellular and exosomal RNAs purified from PNT-2 and PC-3M-luc cells. In the sub-dataset of secretory exosomal miRNAs from PNT-2 cells, we found 40 miRNAs whose cellular amounts were lowered by one-half in PC-3M-luc cells (Table 1). The selected miRNAs expectedly include several types of tumor-suppressive miRNAs, such as miR-15a, miR-200 family, miR-148a, miR-193b, miR-126, and miR-205 (10, 15, 17–20). This observation supports the idea that secretory tumor-suppressive miRNAs are transferred from non-cancerous cells to cancerous cells, in accordance with the concentration gradient of the miRNA.

We have so far demonstrated that normal cells have a higher secretion of tumor-suppressive miRNAs than cancerous cells; however, it remains unclear whether or not these secreted miRNAs affect the proliferation of cells of their origin. To answer this question, we introduced synthesized miR-143 to both PNT-2 and PC-3M-luc cells and assessed their proliferation rates. After 3 days of transfections, the miR-143 analog induced growth inhibition of PC-3M-luc cells compared with mock and control small RNA transfection (Fig. 2*D*, *left panel*). In contrast, the exogenously transduced miR-143 did not show its anti-proliferative effect in PNT-2 cells (Fig. 2*D*, *right panel*), indicating that excessive miR-143 did not confer an additional growth inhibitory effect on normal cells in which expression of miR-143 is maintained to a physiological level. This finding suggests that animal cells may have their own threshold amount for miRNA activity. The different sensitivity found in different cell types can help secretory miRNAs fulfill their purpose to combat exclusively precancerous cells. It is possible that secretory miRNAs, at least, derived from non-cancerous cells such as PNT-2 cells could supplement growth-suppressive signals that are decreased in cancerous cells. Thus, secreted miR-143 might be involved in the cell competitive regulatory system.

TABLE 1

A list of PNT-2-derived secretory miRNAs that were down-regulated less than 0.5-fold in PC-3M cells compared with PNT-2 cells

miRNAs	Fold change[a]
hsa-miR-141	0.0
hsa-miR-200c	0.0
hsa-miR-886–3p	0.0
hsa-miR-30a*	0.0
hsa-miR-155	0.0
hsa-miR-205	0.0
hsa-miR-224	0.0
hsa-miR-148a	0.0
hsa-miR-130a	0.0
hsa-miR-30a	0.1
hsa-miR-663	0.1
hsa-miR-181a-2*	0.1
hsa-miR-484	0.1
hsa-miR-10a	0.1
hsa-miR-192	0.1
hsa-miR-193b	0.1
hsa-miR-200a	0.1
hsa-miR-429	0.1
hsa-miR-769–5p	0.1
hsa-miR-200b	0.2
hsa-miR-195	0.2
hsa-miR-203	0.2
hsa-miR-7	0.2
hsa-miR-200a*	0.2
hsa-miR-200b*	0.2
hsa-miR-30c	0.2
hsa-miR-126	0.3
hsa-miR-149	0.3
hsa-miR-30d	0.3
hsa-miR-181a	0.3
hsa-miR-30e*	0.3
hsa-miR-365	0.4
hsa-miR-135b	0.4
hsa-miR-454*	0.4
hsa-miR-129*	0.4
hsa-miR-30b	0.4
hsa-miR-181b	0.4
hsa-miR-210	0.4
hsa-miR-455–3p	0.5
hsa-miR-15a	0.5

[a] Fold change of the expression of miRNAs in PC-3M cells compared with PNT-2 cells is indicated.

Secretory miR-143 Inhibited Prostate Cancer Cell Proliferation in Vitro—To examine whether miR-143 released from normal cells exert an anti-proliferative activity, we generated HEK293 cells overexpressing miR-143 by nearly 200-fold compared with control (supplemental Fig. 3*A*). After a 3-day incubation with the CM derived from the miR-143-overproducing HEK293 cells and control HEK293 cells, PC-3M-luc cells showed an ~50% decrease in proliferation (Fig. 3*A*, *lanes 1* and *3*). Importantly, the decrease was recovered by the transfection of anti-miR-143 in PC-3M-luc cells (Fig. 3*A*, *lane 3* and *4*). These data indicate that the growth inhibition is attributable to secretory miR-143 contained in the supernatant of miR-143-overexpressing HEK293 cells. In agreement with the exosome-dependent machinery of miRNA secretion, we observed a similar result by using exosome fractions purified from miR-143-transduced HEK293 cells (Fig. 3*B*).

To further study miRNA transfer on a molecular level, we performed a target gene expression analysis and an miRNA-responsive reporter assay. The immunoblotting analysis shows that the addition of the CM isolated from miR-143-overexpressing HEK293 cells significantly knocked down expression of KRAS, a target gene for miR-143 (21), in PC-3M-luc cells (Fig. 3*C*). In addition, we implemented luciferase analyses using

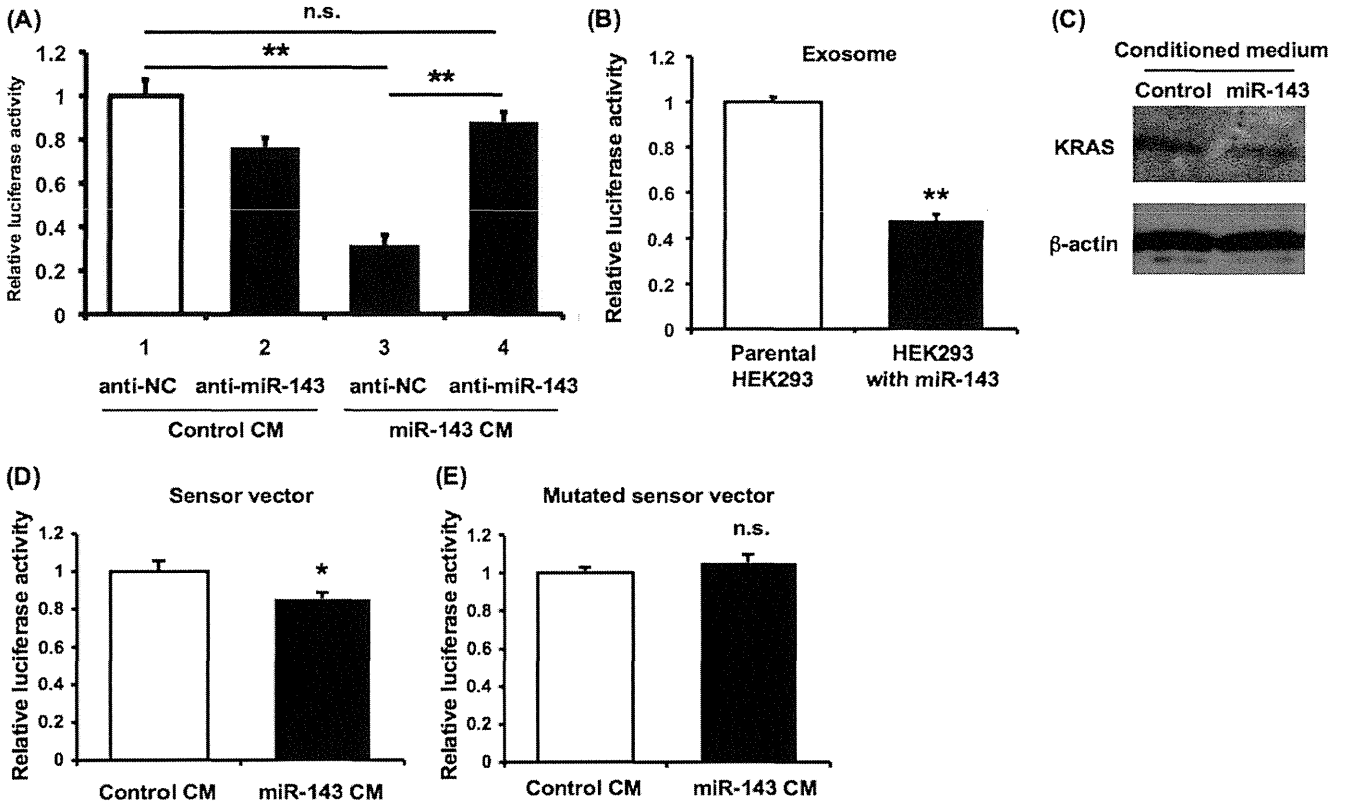

FIGURE 3. **Transfer of secretory miR-143 to PC-3M-luc cells *in vitro*.** *A*, the transfection of anti-miR-143 to PC-3M-luc cells restored the reduced cell growth by the CM derived from miR-143 overproducing cells. After the transfection with 3 nM miR-143 inhibitor molecule (anti-miR-143) (*lanes 2* and *4*) or its control molecule (*anti-NC*) (*lanes 1* and *3*), PC-3M-luc cells were incubated for 3 days in a control conditioned medium (*lanes 1* and *2*) and CM containing extracellular miR-143 (*lane 3* and *4*) followed by a cell growth assay as described under "Experimental Procedures." The values on the *y* axis are depicted relative to the normalized luciferase activity of cells treated in a culture medium, which is defined as 1. Each *bar* is presented as the mean S.E. ($n = 3$). (*, $p < 0.05$; Student's *t* test; *n.s.*, not significant). *B*, cell growth inhibition by exosomes derived from miR-143-transduced HEK293 cells is shown. PC-3M-luc cells were incubated in the exosomes followed by cell growth assay as described under "Experimental Procedures." The values on the *y* axis are depicted relative to the normalized luciferase activity of cells treated with exosomes derived from original HEK293 cells, defined as 1. Each *bar* is presented as the mean S.E. ($n = 3$). (**, $p < 0.005$; Student's *t* test). *C*, secretory miR-143-mediated KRAS suppression in PC-3M-luc cells is shown. Ten micrograms of protein of whole cell lysates prepared from PC-3M-luc cells treated with or without secretory miR-143 were applied to electrophoresis. Immunoblotting was performed with KRAS and actin antibodies and visualized by LAS-3000 system. *D*, extracellular miR-143 derived from HEK293 cells suppressed the luciferase activity of the sensor vector. HEK293 cells transfected with an miR-143 sensor vector were used as recipient cells. The recipient cells were incubated in a CM containing extracellular miRNAs. After a 2-day incubation, a luciferase reporter assay was performed as described under "Experimental Procedures." The values on the *y* axis are depicted relative to the normalized luciferase activity of original HEK293-conditioned medium-treated cells, which is defined as 1. Each *bar* is presented as the mean S.E. ($n = 3$). *, $p < 0.05$; Student's *t* test). *E*, extracellular miR-143 did not reduce the luciferase activity of the mutated sensor vector. HEK293 cells transfected with the mutated miR-143 sensor vector were used as recipient cells. The recipient cells were incubated in a conditioned medium containing extracellular miRNAs. The luciferase assay was carried out as described above. The values on the *y* axis are depicted relative to the normalized renilla luciferase activity of control cells, which is defined as 1. Each *bar* is presented as the mean S.E. ($n = 3$). *n.s.* represents not significant.

a sensor vector harboring renilla luciferase fused in tandem with miR-143 seed sequence in the 3′-UTR. As shown in Fig. 3*D*, the normalized renilla luciferase activities were reduced by the treatment of miR-143-enriched CM derived from HEK293 cells stably expressing miR-143. In contrast, we did not detect any changes of luminescence by using a mutated vector instead of the intact sensor vector (Fig. 3*E*). Furthermore, we quantified cellular amounts of miR-143 in PC-3M-luc cells incubated with CM derived from HEK293 cells or miR-143 overproducing HEK293 cells by QRT-PCR. As shown in supplemental Fig. 3*B*, miR-143 was clearly increased at a cellular level by the treatment of the miR-143 enriched CM. These results indicate that secretory miR-143 exhibits its on-target growth-inhibitory effect in neighboring precancerous cells, thereby suppressing their disordered growth.

Secretory miR-143 Functions as Tumor Suppressor in Vivo—To our knowledge it has never been demonstrated that extracellular tumor-suppressive miRNAs can be transferred into living cells and induce phenotypic change *in vivo*. To address this possibility, we injected CM derived from miR-143 overproducing HEK293 cells or parental HEK293 cells into nude mice implanted with PC-3M-luc cells. Four days after the subcutaneous implantation, we carried out *in vivo* imaging and CM injections according to the timetable shown in Fig. 4*A*. Tumor expansions have been restrained for 8 days with intratumor administrations of miR-143 enriched CM, and consequently the tumor masses shrank by ~0.5-fold on day 8 (Fig. 4*B*). The representative luminescent images of inoculated PC-3M-luc cells on day 8 were shown in Fig. 4*C*. Consistent with the finding that miR-143 did not impair growth activity of non-cancer cells *in vitro* (Fig. 2*D*), no toxicity was observed in these mice (data not shown). In addition, the expressions of miR-143 target genes, such as KRAS and ERK5 (16, 21), were decreased after miR-143-transduced CM injections, indicative of intercellular miRNA transfer *in vivo* (Fig. 4*D*). Thus, our prostate cancer xenograft model suggests that the tumor-suppressive miRNAs

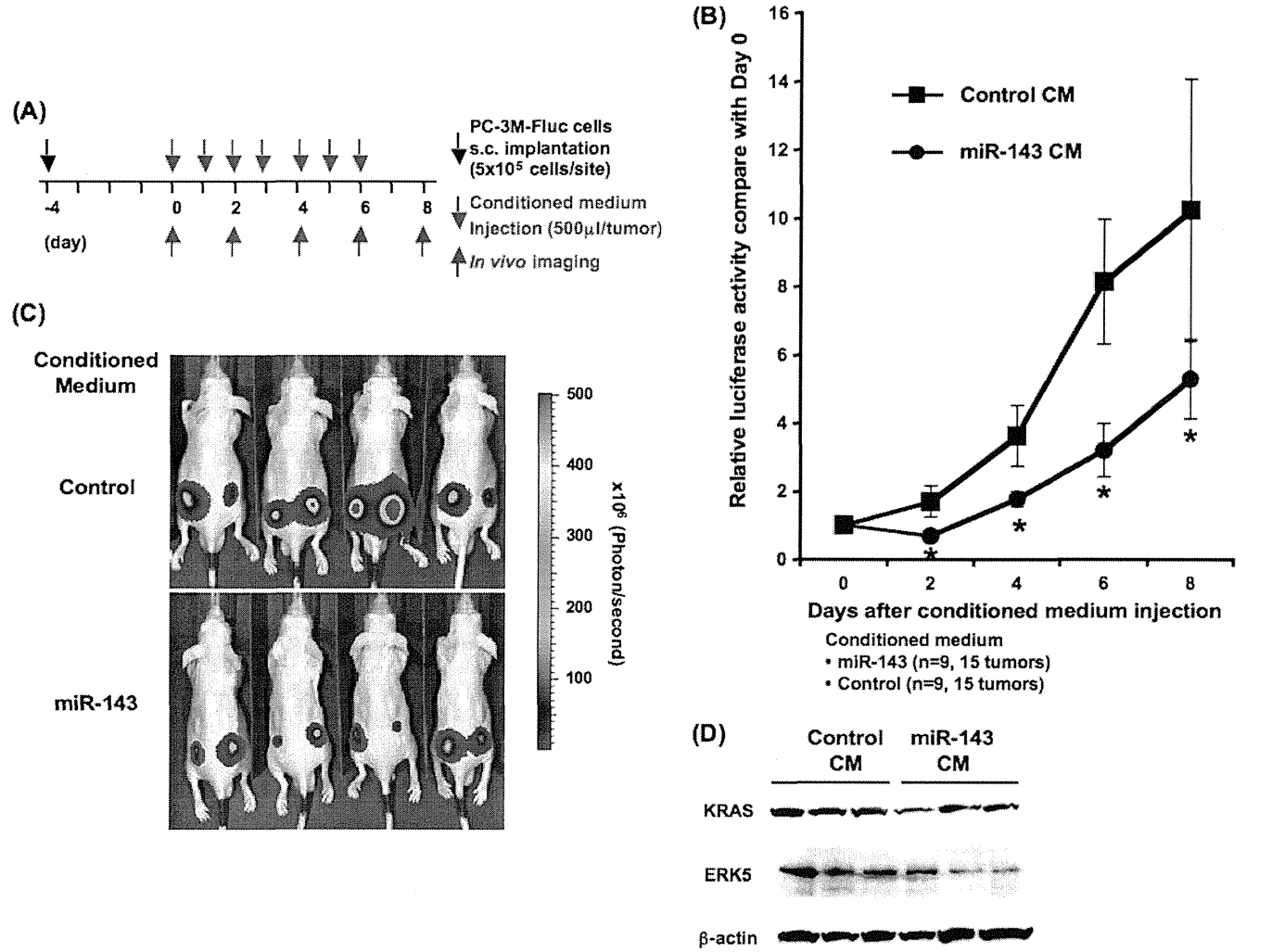

FIGURE 4. **Transfer of secretory miR-143 to PC-3M-luc cells *in vivo*.** *A*, shown is the timetable for conditioned medium injections and *in vivo* imaging. *B*, shown are tumor growth ratios of the inoculated PC-3M-luc cells during the secretory miR-143 treatment. *Closed circles* and *closed squares* indicate the tumor mass administrated with CM from miR-143-overproducing HEK293 cells or parental HEK293 cells, respectively. The values on the *y* axis are depicted relative to the luciferase activity of each tumor on day 0, which is defined as 1. Each *bar* is presented as the mean S.E. ($n = 9$). *, $p < 0.05$; Student's *t* test. *C*, representative images are shown of tumor cells in the skin of mice. Bioluminescence of firefly luciferase from miR-143-enriched CM treated mice and control mice were detected on day 8 with IVIS imaging system. *D*, shown is secretory miR-143-mediated KRAS and ERK5 suppression in inoculated tumor cells. On day 8 the inoculated tumor masses were isolated and applied to immunoblotting analysis for the quantification of KRAS and ERK5 on a protein level.

secreted from normal cells could be efficiently delivered into their neighboring tumors *in vivo*.

DISCUSSION

In this study we documented that miR-143 derived from non-cancerous cells had the ability to suppress the growth of cancer cell proliferation not only *in vitro* but also *in vivo*. These observations suggest that tumor-suppressive miRNAs can be implicated in cell competition between cancer cells and non-cancer cells. In this context, normal cells attempt to prevent the outgrowth of precancerous cells by secreting anti-proliferative miRNAs and maintain a healthy condition; however, the abnormal cells can circumvent this inhibitory machinery, finally resulting in a tumor expansion (Fig. 2*A*). Cell competition could be a homeostatic mechanism that tumor cells need to overcome (1).

Here, we discuss two possible mechanisms by which cancer cells can gain resistance to secretory tumor-suppressive miRNAs. One is a blockade for the uptake of miRNAs, and the other is a cancellation of silencing activity of the incorporated miRNAs. As previously reported, miRNAs are loaded into exosomes and then secreted from living cells (7, 22, 23). If exosomes enriched in miRNAs are actively incorporated by recipient cells, cancer cells can impair the uptake mechanism to escape from the attack of secretory tumor-suppressive miRNAs. This scenario is supported by a recent publication regarding a Tim4 expected for an exosome receptor (24).

In the latter case cancer cells need to specifically compromise the incorporated tumor-suppressive miRNAs because there are some types of miRNAs that are indispensable for the expansion of cancer cells. A RISC assembly is composed of many protein families, such as the mammalian AGO family, GW182, and heat shock proteins (25). Moreover, each gene family also consists of many members, thereby generating diversity of RISC assemblies. The heterogeneity of RISC assemblies allows tumor-suppressive miRNAs to selectively bind with a RISC and silence their target genes on the complex. If cancer cells can exclusively destroy the tumor-suppressive RISC assembly, they can safely

grow in a limited niche full of anti-proliferative miRNAs. The detailed mechanism of the resistance to cell competition remains unknown.

In addition to the acquired resistance, there is another possibility that normal cells will lose secretory capacity of exosomal miRNAs. p53 was shown to enhance exosome production in cells undergoing a p53 response to stress (26). In other words, dysfunction of p53 will result in decreased miRNA secretion. The tumor-suppressive ability of p53 can partly depend on the control of miRNA release from normal cells.

Numerous studies show a broad variety of reasons for tumor initiation, including gene amplification, cellular stress, metabolic alteration, and epigenetic changes. This work suggests that the disruption of the cell competitive process mediated by secretory miRNAs will result in the occurrence of neoplasm. Understanding the mechanism by which homeostasis is impaired leads to a novel therapeutic approach for cancer progression.

Acknowledgments—We thank Katsuyuki Hayashi and Ikuei Hiraka at DNA Chip Research Inc. for supporting the processing of microarray data. We thank Ayako Inoue for excellent technical assistance.

REFERENCES

1. Johnston, L. A. (2009) Competitive interactions between cells: death, growth, and geography. *Science* **324,** 1679–1682
2. Díaz, B., and Moreno, E. (2005) The competitive nature of cells. *Exp. Cell Res.* **306,** 317–322
3. Hanahan, D., and Weinberg, R. A. (2011) Hallmarks of cancer. The next generation. *Cell* **144,** 646–674
4. Bondar, T., and Medzhitov, R. (2010) p53-mediated hematopoietic stem and progenitor cell competition. *Cell Stem Cell* **6,** 309–322
5. Dong-Le Bourhis, X., Berthois, Y., Millot, G., Degeorges, A., Sylvi, M., Martin, P. M., and Calvo, F. (1997) Effect of stromal and epithelial cells derived from normal and timorous breast tissue on the proliferation of human breast cancer cell lines in co-culture. *Int. J. Cancer* **71,** 42–48
6. Senoo-Matsuda, N., and Johnston, L. A. (2007) Soluble factors mediate competitive and cooperative interactions between cells expressing different levels of *Drosophila* Myc. *Proc. Natl. Acad. Sci. U.S.A.* **104,** 18543–18548
7. Kosaka, N., Iguchi, H., Yoshioka, Y., Takeshita, F., Matsuki, Y., and Ochiya, T. (2010) Secretory mechanisms and intercellular transfer of microRNAs in living cells. *J. Biol. Chem.* **285,** 17442–17452
8. Croce, C. M. (2009) Causes and consequences of microRNA dysregulation in cancer. *Nat. Rev. Genet.* **10,** 704–714
9. Suzuki, H. I., Yamagata, K., Sugimoto, K., Iwamoto, T., Kato, S., and Miyazono, K. (2009) Modulation of microRNA processing by p53. *Nature* **460,** 529–533
10. Takeshita, F., Patrawala, L., Osaki, M., Takahashi, R. U., Yamamoto, Y., Kosaka, N., Kawamata, M., Kelnar, K., Bader, A. G., Brown, D., and Ochiya, T. (2010) Systemic delivery of synthetic microRNA-16 inhibits the growth of metastatic prostate tumors via down-regulation of multiple cell-cycle genes. *Mol. Ther.* **18,** 181–187
11. Peng, X., Guo, W., Liu, T., Wang, X., Tu, X., Xiong, D., Chen, S., Lai, Y., Du, H., Chen, G., Liu, G., Tang, Y., Huang, S., and Zou, X. (2011) Identification of miRs-143 and -145 that is associated with bone metastasis of prostate cancer and involved in the regulation of EMT. *PLoS One* **6,** e20341
12. Franses, J. W., Baker, A. B., Chitalia, V. C., and Edelman, E. R. (2011) *Sci. Transl. Med.* **3,** 66ra65
13. Savina, A., Vidal, M., and Colombo, M. I. (2002) The exosome pathway in K562 cells by Rab11. *J. Cell Sci.* **115,** 2505–2515
14. Trajkovic, K., Hsu, C., Chiantia, S., Rajendran, L., Wenzel, D., Wieland, F., Schwille, P., Brügger, B., and Simons, M. (2008) Ceramide triggers budding of exosome vesicles into multivesicular endosomes. *Science* **319,** 1244–1247
15. Gandellini, P., Folini, M., Longoni, N., Pennati, M., Binda, M., Colecchia, M., Salvioni, R., Supino, R., Moretti, R., Limonta, P., Valdagni, R., Daidone, M. G., and Zaffaroni, N. (2009) miR-205 exerts tumor-suppressive functions in human prostate through down-regulation of protein kinase Cepsilon. *Cancer Res.* **69,** 2287–2295
16. Clapé, C., Fritz, V., Henriquet, C., Apparailly, F., Fernandez, P. L., Iborra, F., Avancès, C., Villalba, M., Culine, S., and Fajas, L. (2009) miR-143 interferes with ERK5 signaling and abrogates prostate cancer progression in mice. *PLoS One* **4,** e7542
17. Kong, D., Li, Y., Wang, Z., Banerjee, S., Ahmad, A., Kim, H. R., and Sarkar, F. H. (2009) miR-200 regulates PDGF-D-mediated epithelial-mesenchymal transition, adhesion, and invasion of prostate cancer cells. *Stem Cells* **27,** 1712–1721
18. Fujita, Y., Kojima, K., Ohhashi, R., Hamada, N., Nozawa, Y., Kitamoto, A., Sato, A., Kondo, S., Kojima, T., Deguchi, T., and Ito, M. (2010) MiR-148a attenuates paclitaxel resistance of hormone-refractory, drug-resistant prostate cancer PC3 cells by regulating MSK1 expression. *J. Biol. Chem.* **285,** 19076–19084
19. Saito, Y., Friedman, J. M., Chihara, Y., Egger, G., Chuang, J. C., and Liang, G. (2009) Epigenetic therapy up-regulates the tumor suppressor microRNA-126 and its host gene EGFL7 in human cancer cells. *Biochem. Biophys. Res. Commun.* **379,** 726–731
20. Rauhala, H. E., Jalava, S. E., Isotalo, J., Bracken, H., Lehmusvaara, S., Tammela, T. L., Oja, H., and Visakorpi, T. (2010) miR-193b is an epigenetically regulated putative tumor suppressor in prostate cancer. *Int. J. Cancer* **127,** 1363–1372
21. Xu, B., Niu, X., Zhang, X., Tao, J., Wu, D., Wang, Z., Li, P., Zhang, W., Wu, H., Feng, N., Wang, Z., Hua, L., and Wang, X. (2011) miR-143 decreases prostate cancer cells proliferation and migration and enhances their sensitivity to docetaxel through suppression of KRAS. *Mol. Cell Biochem.* **350,** 207–213
22. Gibbings, D. J., Ciaudo, C., Erhardt, M., and Voinnet, O. (2009) Multivesicular bodies associate with components of miRNA effector complexes and modulate miRNA activity. *Nat. Cell Biol.* **11,** 1143–1149
23. Pegtel, D. M., Cosmopoulos, K., Thorley-Lawson, D. A., van Eijndhoven, M. A., Hopmans, E. S., Lindenberg, J. L., de Gruijl, T. D., Würdinger, T., and Middeldorp, J. M. (2010) Functional delivery of viral miRNAs via exosomes. *Proc. Natl. Acad. Sci. U.S.A.* **107,** 6328–6333
24. Miyanishi, M., Tada, K., Koike, M., Uchiyama, Y., Kitamura, T., and Nagata, S. (2007) Identification of Tim4 as a phosphatidylserine receptor. *Nature* **450,** 435–439
25. Kwak, P. B., Iwasaki, S., and Tomari, Y. (2010) The microRNA pathway and cancer. *Cancer Sci.* **101,** 2309–2315
26. Yu, X., Harris, S. L., and Levine, A. J. (2006) The regulation of exosome secretion. A novel function of the p53 protein. *Cancer Res.* **66,** 4795–4801

THE JOURNAL OF BIOLOGICAL CHEMISTRY VOL. 287, NO. 41, pp. 34110–34119, October 5, 2012

Micromanaging Iron Homeostasis

HYPOXIA-INDUCIBLE MICRO-RNA-210 SUPPRESSES IRON HOMEOSTASIS-RELATED PROTEINS[*S]

Received for publication, February 27, 2012, and in revised form, August 14, 2012 Published, JBC Papers in Press, August 15, 2012, DOI 10.1074/jbc.M112.356717

Yusuke Yoshioka[‡§1], **Nobuyoshi Kosaka**[§], **Takahiro Ochiya**[§], **and Takashi Kato**[‡¶2]

From the [‡]*Integrative Bioscience and Biomedical Engineering, Graduate School of Science and Engineering, Waseda University, 2-2 Wakamatsu, Shinjuku, Tokyo 162-8480, Japan, the* [§]*Translational Research Group Division of Molecular and Cellular Medicine, National Cancer Center Research Institute, 5-1-1 Tsukiji, Chuo-ku, Tokyo 104-0045, Japan, and the* [¶]*Department of Biology, School of Education, Waseda University, Tokyo 162-8480, Japan*

Background: The regulatory mechanisms of iron homeostasis in cancer cells are not yet fully understood.
Results: MicroRNA-210 suppresses two essential molecules for iron homeostasis, TfR and ISCU.
Conclusion: Precise regulation of microRNA-210 expression level is vital for maintaining the iron homeostasis, leading to the survival of cancer cells.
Significance: This study reveals the linkages among hypoxia, iron homeostasis, and cancer.

Iron is fundamental for sustaining life for living organisms, and the iron metabolism is finely regulated at different levels. In cancer cells, deregulation of the iron metabolism induces oxidative stress and drives tumor progression and metastasis; however, the molecular mechanisms of iron homeostasis are not fully understood. Here we found that iron deficiency as well as hypoxia promoted microRNA-210 (miR-210) expression. A central mediator of miR-210 transcriptional activation is the hypoxia-inducible factor (HIF)-1α, and the hypoxia-response element in the miR-210 promoter is confirmed experimentally. This is in agreement with the data from *in vivo* studies that have demonstrated the presence of miR-210-expressing cells at the chronic hypoxic regions of xenografted tumors. Furthermore we found two essential molecules for iron homeostasis, iron-sulfur cluster scaffold protein (ISCU) and transferrin receptor 1 (TfR), are a direct target of miR-210. Transfection of miR-210 decreases the uptake of transferrin by inhibiting the expression of TfR. In addition, inhibition of miR-210 by anti-miR-210 up-regulates ISCU expression. These findings suggest that miR-210 works as an iron sensor and is involved in the maintenance of iron homeostasis by sustaining the TfR expression level to stimulate cell proliferation and promote cell survival in the hypoxic region within tumors.

During the evolutionary processes, life has made use of iron in a variety of biochemical processes. For instance, iron is an essential cofactor for nonheme enzymes, such as ribonucleotide reductase, which is essential for DNA synthesis and is also a vital component of the heme in the oxygen-binding protein, hemoglobin (1–3). Iron needs to be tightly regulated, as excess iron is toxic and causes the generation of free radicals (4), whereas iron insufficiency induces hypoferric anemia in mammals (5) coupled to hypoxia in tissues (6, 7). Given the links between iron metabolism and oxygen transport, the associations between the control of the iron concentration and the physiology of the hypoxic response are important (8). Many responses to altered oxygen levels are coordinated by a hypoxia-inducible factor (HIF)[3] (9, 10).

The association between iron and cancer has been shown in animal models and epidemiologic studies in several human cancers. For instance, the oldest reported experiment of iron-induced carcinogenesis is that of mice exposed to iron-oxide dust, which caused pulmonary tumors (11). In addition, various studies have also shown higher levels of expression of the transferrin receptor 1 (TfR), which is an essential protein involved in iron uptake and the regulation of cell growth, in cancer cells than in their normal counterparts (12). TfR could be attributed to the increased need for iron as a cofactor of ribonucleotide reductase involved in the DNA synthesis of rapidly dividing cells. These reports suggest that iron homeostasis is important in cancer initiation and progression. However, the regulatory mechanisms of iron homeostasis in cancer cells are not yet fully understood.

MicroRNAs (miRNAs) have emerged as a new class of non-coding genes involved in regulating a wide variety of biological processes (13, 14), and their mis-expression has been shown to contribute to tumorigenesis (15). Therefore, miRNAs act as

* This work was supported in part by a grant-in-aid for the third-term comprehensive 10-year strategy for cancer control, a grant-in-aid for scientific research on priority areas cancer from the Ministry of Education, Culture, Sports, Science, and Technology, and the Program for Promotion of Fundamental Studies in Health Sciences of the National Institute of Biomedical Innovation (NiBio), the Japan Society for the Promotion of Science (JSPS) through the "Funding Program for World-Leading Innovative R&D on Science and Technology (FIRST Program)," initiated by the Council for Science and Technology Policy (CSTP). This work was supported in part by a grant from the Japan Society for the Promotion of Science (to Y. Y.).
[S] This article contains supplemental Figs. S1–S7.
[1] Supported by a Research Fellowship of the Japan Society for the Promotion of Science for Young Scientists.
[2] To whom correspondence should be addressed: Department of Biology, School of Education and Molecular Physiology Unit Major in Integrative Bioscience and Biomedical Engineering, Graduate School of Science and Engineering, 2-2 Wakamatsu, Shinjuku, Tokyo 162-8480, Japan. Tel.: 81-3-5369-7309; Fax: 81-3-3355-0316; E-mail: tkato@waseda.jp.

[3] The abbreviations used are: HIF, hypoxia-inducible factor; Tf, transferrin; TfR, transferrin receptor 1; miRNA, microRNA; miRNA-210, microRNA-210; ISCU, iron-sulfur cluster scaffold protein; DFO, desferrioxamine; qRT-PCR, quantitative real-time RT-PCR; IRP1, iron regulatory protein 1; NC, negative control.

tuners of gene expression and maintain homeostasis. For instance, miR-144/451 knockout mice display a cell autonomous impairment of late erythroblast maturation, resulting in erythroid hyperplasia, splenomegaly, and mild anemia (16).

In a previous report, we demonstrated that miR-210 is highly expressed in human and murine erythroid cells and in the spleen of mice with hemolytic anemia (17). Erythrocytes require iron to perform their duty as oxygen carriers. Recent reports have shown that the expression of miR-210 is induced by hypoxic conditions (18). Therefore, miR-210 might play an important role in the connection of iron and oxygen. It was already reported that the expression of miR-210 was tightly associated with poor prognosis of breast cancer (18); however, contradictory data exist concerning the regulation and roles of miR-210 during cancer progression. In this study, we clarified that miR-210 regulates iron homeostasis in cancer cells. The expression of miR-210 was induced not only in hypoxic conditions but also in iron deficiency. In addition, we found that the targets of miR-210 are two essential molecules for iron homeostasis, TfR and the iron-sulfur cluster scaffold protein (ISCU). Furthermore, we showed that the distribution of miR-210-expressing cells in inoculated tumor cells could be observed in the chronic hypoxic regions. These results indicated that iron-deficiency-inducible miR-210 controls the expression of two iron regulatory proteins to optimize the survival and proliferation rate of cancer cells located in the chronic hypoxic regions.

EXPERIMENTAL PROCEDURES

Reagents—Rabbit polyclonal anti-ISCU (FL-142) (sc-28860) was purchased from Santa Cruz Biotechnology (Santa Cruz, CA). Mouse monoclonal anti-TfR (13-6800) was purchased from Invitrogen. Mouse monoclonal anti-actin, clone C4 (MAB1501), was purchased from Millipore (Billerica, MA). Mouse monoclonal anti-HIF-1α (610959) was purchased from BD Biosciences. Rabbit monoclonal anti-ferritin (EPR3004Y) was purchased from Epitomics (Burlingame, CA). Rabbit polyclonal anti-ACO1/iron regulatory protein 1 (IRP1) was purchased from Medical & Biological Laboratories Co., Ltd. Rabbit polyclonal anti-red fluorescent protein (ab34771) was purchased from Abcam (Cambridge, MA). Peroxidase-labeled anti-mouse and anti-rabbit antibodies were included in the Amersham Biosciences ECL Plus Western blotting reagents pack (RPN2124) (GE Healthcare). Synthetic hsa-miR-210 (pre-miR-210) and antisense miR-210 oligonucleotide (anti-miR-210) were purchased from Ambion (Austin, TX). The duplexes of each small interfering RNA (siRNA) targeting human HIF-1α mRNA (s30925; target sequences of 5′-GGAGGUGUUUGACAAGCGAdTdT-3′ and 5′-UCGCUUGUCAAACACCUCCtg-3′), an siRNA-specific for human IRP1 (ACO1) mRNA (target sequences of 5′-GCUCGCUACUUAACUAACAtt-3′ and 5′-UGUUAGUUAAGUAGCGAGCag-3′) and negative control 1 (NC1) were purchased from Applied Biosystems. An siRNA-specific for human TfR mRNA (target sequences of 5′-GAACCUGGAUAAUGAUGAAdTdT-3′ and 5′-UUCAUCAUUAUCCAGGUUCdTdT-3′) was purchased from Sigma-Genosys. Desferrioxamine (DFO) was purchased from Calbiochem. Geneticin was purchased from Invitrogen.

Cell Culture—MCF7 cells and MD-MB-231-luc-D3H2LN cells (Xenogen), a human breast cancer cell line, were cultured in RPMI 1640 medium containing 10% heat-inactivated fetal bovine serum (FBS) and an antibiotic-antimycotic (Invitrogen) at 37 °C in 5% CO_2.

Exposure to Hypoxia—Cells were exposed for 24 h or 48 h either to standard nonhypoxic cell culture conditions (20% O_2, 5% CO_2 at 37 °C) or to hypoxia (1% O_2, 5% CO_2 with N_2 balance at 37 °C) in either a modular hypoxia chamber (Wakenyaku) or a tissue culture incubator.

RNA Extraction—RNA was isolated using TRIzol (Invitrogen) and processed according to the manufacturer's instructions.

Quantitative Real-time RT-PCR (qRT-PCR)—Hsa-miR-210 and endogenous control RNU6B TaqMan qRT-PCR kits and human-ISCU, human-TfR, and human-β-actin TaqMan Gene Expression Assays were purchased from Applied Biosystems (Foster City, CA). The reverse transcription and TaqMan quantitative PCR were performed according to the manufacturer's instructions. PCR was carried out in 96-well plates using the 7300 Real-Time PCR System (Applied Biosystems). All reactions were done in triplicate.

The expression levels of pri-miR-210 and β-actin were measured by qRT-PCR using a SYBR Green PCR Master Mix (Invitrogen). Primer sequences are as follows (shown 5′ to 3′): pri-miRNA-210_F, GACTGGCCTTTGGAAGCTCC and R, ACAGCCTTTCTCAGGTGCAG; β-actin_F, GGCACCACCATGTACCCTG and R, CACGGAGTACTTGCGCTCAG.

In Silico MicroRNA Target Prediction—Bioinformatic prediction of target genes and miRNA-binding sites was performed using three programs: TargetScan (version 5.0) (19), Sanger miRBase (version 5) (20), and MirTarget2 (21).

3′-UTR Assay Plasmid Constructs—A 297-bp fragment from the 3′-UTR of ISCU containing the predicted target sequence of miR-210 (located at positions 102–109 of the ISCU1/2 3′-UTR) and a 385-bp fragment from the 3′-UTR of TfR containing the predicted target sequence of miR-210 (located at positions 229–235 of this fragment) were PCR-cloned from MCF7-isolated total RNA. Three prime A-overhang was added to the PCR products after 15 min of regular *Taq* polymerase treatment at 72 °C. The PCR products were cloned into a pGEM-T Easy Vector (Promega; Madison, WI). A pair of primers including XhoI and NotI restriction sites was designed to amplify the 3′-UTR of ISCU and TfR insert. The amplified products were ligated into the XhoI and NotI sites of the 3′-UTR of the *Renilla* luciferase gene in the psi-check-2 plasmid (Promega) to generate psi-ISCU and psi-TfR. Primer sequences are as follows (shown 5′ to 3′): ISCU_F, GCTCGAGTAACTCCGTTACTTCCAGCAGGC and ISCU_R, GCGGCCGCTAATATGCACTTCACGGGCTATC; TfR_F, GCTCGAGTAATCAGCTGTTTGTCATAGGGC and TfR_R, GCGGCCGCTAGGTCATGCACGATTGTCCGA. Site-directed mutagenesis or deletion mutant was performed in the seed sequences of ISCU and TfR. PrimeStar Max DNA Polymerase (Takara; Kyoto, Japan) was used for PCR amplification. Forward primer and reverse primer sequences are as follows (shown 5′ to 3′): ISCU_mut_F, AGATGTATGTGGTACTTGCTGTTCACGTTA and ISCU_mut_R, GTACCACATACAT-

CTCATAGCTCTTCGGT; ISCU_del_F, ATGAGATTACTTGCTGTTCACGTTA and ISCU_del_R, GCAAGTAATCTCATAGCTCTTCGGT; TfR_mut_F, TGTTGCACGCGCGTACTTAAATGAAAGCA and TfR_mut_R, TACGCGCGTGCAACACCCGAACCAGGAAT; TfR_del_F, CGGGTGTTCGTACTTAAATGAAAGCA and TfR_del_R, AAGTACGAACACCCGAACCAGGAAT.

Immunoblot Analysis—SDS-PAGE gels were calibrated with Precision Plus Protein standards (161-0375) (Bio-Rad), and anti-HIF-1α (1:500), anti-ISCU (1:200), anti-TfR (1:500), and anti-actin (1:1000) were used as primary antibodies. The dilution ratio of each antibody is indicated in parentheses. Two secondary antibodies (peroxidase-labeled anti-mouse and anti-rabbit antibodies) were each used at a dilution of 1:10,000. Bound antibodies were visualized by chemiluminescence using the ECL Plus Western blotting detection system (RPN2132) (GE Healthcare), and luminescent images were analyzed with a LuminoImager (LAS-3000; Fuji Film Inc.).

Flow Cytometric Analysis—MCF7 cells and MDA-MB-231-luc-D3H2LN cells were transfected with pre-miR-210 or pre-NC. After culturing for 48 h, transfected cells were serum-starved for 30 min and then incubated for 45 min in a serum-free medium containing 50 μg of transferrin/ml conjugated with Alexa Fluor 594 (Invitrogen). Transfected cells were suspended in their culture medium and subjected to a FACSAria II cell sorter (BD Biosciences). At least one million cells were pelleted by centrifugation at 180 $\times$ *g* for 5 min at 4 °C, resuspended in a 20 μl of a monoclonal mouse anti-human CD71-FITC antibody (BD Biosciences, clone M-A712), and incubated for 30 min at 4 °C. Three independent experiments were performed.

Transferrin-uptake Analysis—Transferrin-uptake experiments were performed 48 h after transfection with pre-miR-210 or pre-NC. Transfected cells were serum-starved for 30 min and then incubated for 45 min in a serum-free medium containing 50 μg of transferrin/ml conjugated with Alexa Fluor 594. Cells were then washed and fixed in 4% paraformaldehyde for 15 min at room temperature. After washing with PBS, they were incubated with mouse anti-TfR antibody diluted 1:100 in Dako REAL Antibody Diluent (Dako; Carpinteria, CA) for 1 h. They were then incubated with Alexa Fluor 488 goat anti-mouse IgG diluted 1:1000 in Dako REAL Antibody Diluent for 45 min. Finally, the cells were stained with the fluorescent DNA-binding dye Hoechst 33342 (Invitrogen) for 5 min.

Establishment of Stable Cell Lines—Stable knockdown of ISCU MCF7 cell lines was generated by selection with 4 μg/ml blasticidine (Invitrogen). MCF7 cells were transfected with 0.5 mg of an siISCU1/2 vector or a negative control vector at 90% confluence in 24-well dishes using a Lipofectamine LTX reagent in accordance with the manufacturer's instructions. After 24 h, the cells were replated in a 10-cm dish followed by 3-week selection with 4 μg/ml blasticidine.

Immunohistochemical Staining—Between all consecutive steps of the staining procedure, the sections were rinsed three times for 5 min in PBS. The sections were first fixed in 10% formalin for 4 h. After re-hydration of the tissue sections in PBS for 1 h, they were incubated with mouse anti-HIF-1α diluted 1:500 and rabbit anti-red fluorescent protein diluted 1:100 in Dako REAL Antibody Diluent for 1 h. Sections were then incubated with Alexa Fluor 488 goat anti-mouse IgG and Alexa Fluor 594 goat anti-rabbit IgG (Molecular Probes; Leiden, The Netherlands) diluted 1:1000 in Dako REAL Antibody Diluent for 45 min. Finally, sections were mounted on ProLong Gold antifade reagent with DAPI (Invitrogen).

In Vivo miR-210-monitoring Assay—The pDsRed-Express-DR vector (Clontech Laboratories), which is a promoterless vector that encodes DsRed-Express-DR, was purchased from Takara Bio. This protein is a destabilized variant of the red fluorescent protein. For miR-210 promoter-driven fluorescent-based reporter assays, pmiR-210-DsRed was constructed by inserting a miR-210 promoter region into a multi-cloning site of pDsRed-Express-DR vector at HindIII and XhoI sites. A sensor vector for miR-210 was constructed by introducing tandem binding sites with a perfect complementarity sequence to miR-210, separated by a four-nucleotide spacer into the NotI site of pDsRed-Express-DR vector, which already introduced the CMV promoter into the multi-cloning site. The sequences of the binding site are as follows: 5′-AGTGATTCAGCCGCTGTCAC***ACGCACA***GACGCGTTCAGCCGCTGTCAC***ACGCACA***GATCGAA-3′ (sense) and 5′-TTCGATC***TGTGCGT***GTGACAGCGGCTGAACGCGTC***TGTGCGT***GTGACAGCGGCTGAATCACT-3′ (antisense). The seed sequence of miR-210 is indicated in bold italics. All plasmids were verified by DNA sequencing.

Statistical Analysis—Data presented as *bar graphs* are the means $\pm$S.E. of at least three independent experiments. Statistical analysis was performed using Student's *t* test.

RESULTS

Iron Deficiency Induces the Expression of miR-210 through the HIF-1α, and miR-210 Directly Suppresses ISCU—To try to determine the possible contribution of miR-210 in the regulation of iron homeostasis, we first measured the expression of miR-210 in breast cancer cells, MCF7 and MDA-MB-231 (MM231) cells, and human breast epithelial cells, MCF10A, after treatment with an iron chelator, DFO. The expression level of miR-210 was increased 3–5-fold above basal levels by the 48 h of DFO treatment compared with untreated cells (Fig. 1*A*). In addition, excess amounts of iron by addition of 500 mM ferric ammonium citrate had no effect on the induction or suppression of the expression of miR-210. To further analyze whether the biogenesis of miR-210 during iron depletion is regulated by a transcriptional mechanism or processing machinery of miRNA biogenesis, we quantified the expression of primary miR-210 (pri-miR-210) in MCF7 cells. The expression of pri-miR-210 levels was induced 1.5–3.5-fold above basal levels by the DFO treatment compared with untreated cells (Fig. 1*B*). This result indicated that the induction of miR-210 is because of transcriptional regulation. As shown previously, the transcription of miR-210 was regulated by iron-deficient-induced HIF-1α through the binding of hypoxia-responsible elements that are located upstream of the miR-210 gene (22) (supplemental Fig. S1, *A–D*). Indeed, suppression of HIF-1α by siRNA (supplemental Fig. S1*E*) leads to a significant reduction of miR-210 expression after treatment with DFO (Fig. 1*C*).

Recent reports showed that miRNAs play a role in feedback and feed-forward transcriptional regulation (23, 24). Previ-

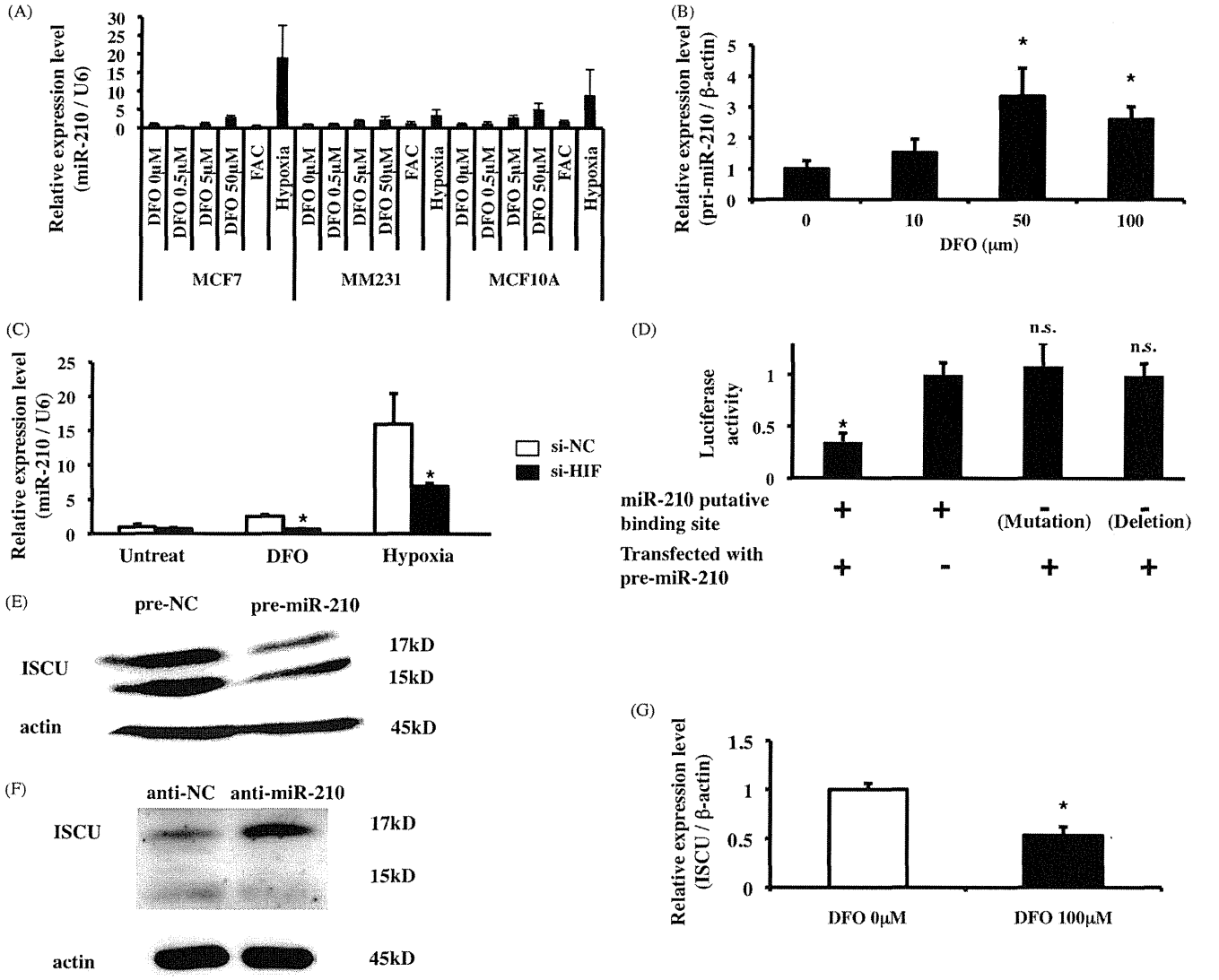

FIGURE 1. **Expression of miR-210 is induced by iron deficiency, and target gene of miR-210 is ISCU.** *A*, miR-210 expression was detected by qRT-PCR after treatment with various concentrations of DFO or exposure to 1% O_2 for 48 h. RNU6B was used as a control. *B*, primary miR-210 expression was detected by qRT-PCR after treatment with DFO for 48 h. β-Actin was used as a control. *C*, MCF7 cells were transfected with HIF-1α siRNA or control siRNA and treatment with DFO 50 μM or exposure to 1% O_2 for 24 h. miR-210 expression was detected by qRT-PCR. RNU6B was used as a control. *, $p < 0.05$ compared with control siRNA groups. *D*, MCF7 cells were co-transfected with pre-miR-210 or pre-NC and psi-ISCU or with its mutant or deletion vector. After 48 h, luciferase activities were measured. *, $p < 0.05$ compared with pre-NC. *n.s.*, not significant. *E*, MCF7 cells were transfected with pre-miR-210 or pre-NC. After 48 h, ISCU expression was detected by immunoblotting. Actin was used as a loading control. *F*, MCF7 cells were transfected with anti-miR-210 or anti-NC and exposed to 1% O_2. After 48 h, ISCU expression was detected by immunoblotting. Actin was used as a loading control. *G*, ISCU expression was detected by qRT-PCR after treatment with DFO 100 μM for 48 h. *, $p < 0.05$ compared with untreated cells. β-Actin was used as a control.

ously, we reported that miR-210 is involved in the production of erythrocytes, which consume 70% of body iron in humans and are the major carriers of oxygen (17, 25). Based on those reports and our finding that the expression of miR-210 was regulated by the iron concentration through the activation of HIF-1α in this study (Fig. 1, *A–C*, and supplemental Fig. S1), we hypothesized that miR-210 regulates genes that are associated with a potent iron homeostasis and a hypoxic cellular response. According to these criteria, ISCU was predicted as a miR-210 target by miRNA target prediction algorithm programs (supplemental Fig. S2*A*). ISCU is an essential factor of the mitochondria electron transport chain, and loss of function of ISCU can disrupt iron homeostasis (26). Although ISCU was known to be regulated by miR-210 in hypoxic condition (27, 28), the precise mechanism of miR-210 on iron homeostasis in cancer cells has not been clarified yet. As shown in Fig. 1*D*, miR-210 recognized the 3′-UTR of ISCU. On the contrary, miR-210 seed sequence in the 3′-UTR of ISCU was mutated or deleted, miR-210 could not bind to the 3′-UTR of ISCU (Fig. 1*D*). In addition, overexpression or knockdown of miR-210 in MCF7 cells down-regulated or up-regulated the expression of ISCU assessed by qRT-PCR (supplemental Fig. S2, *C* and *D*) and immunoblotting (Fig. 1, *E* and *F*). These results are consistent with previous findings that ISCU was a direct target of miR-210. To understand the contribution of miR-210 and ISCU on iron homeostasis in breast cancer cells, we checked the expression of ISCU under the condition of iron depletion in breast cancer cells. As shown in Fig. 1*G*, the expression of ISCU was down-regulated after the treatment with DFO, suggesting that the expression of ISCU was controlled by iron-deficient-induced miR-210 in breast

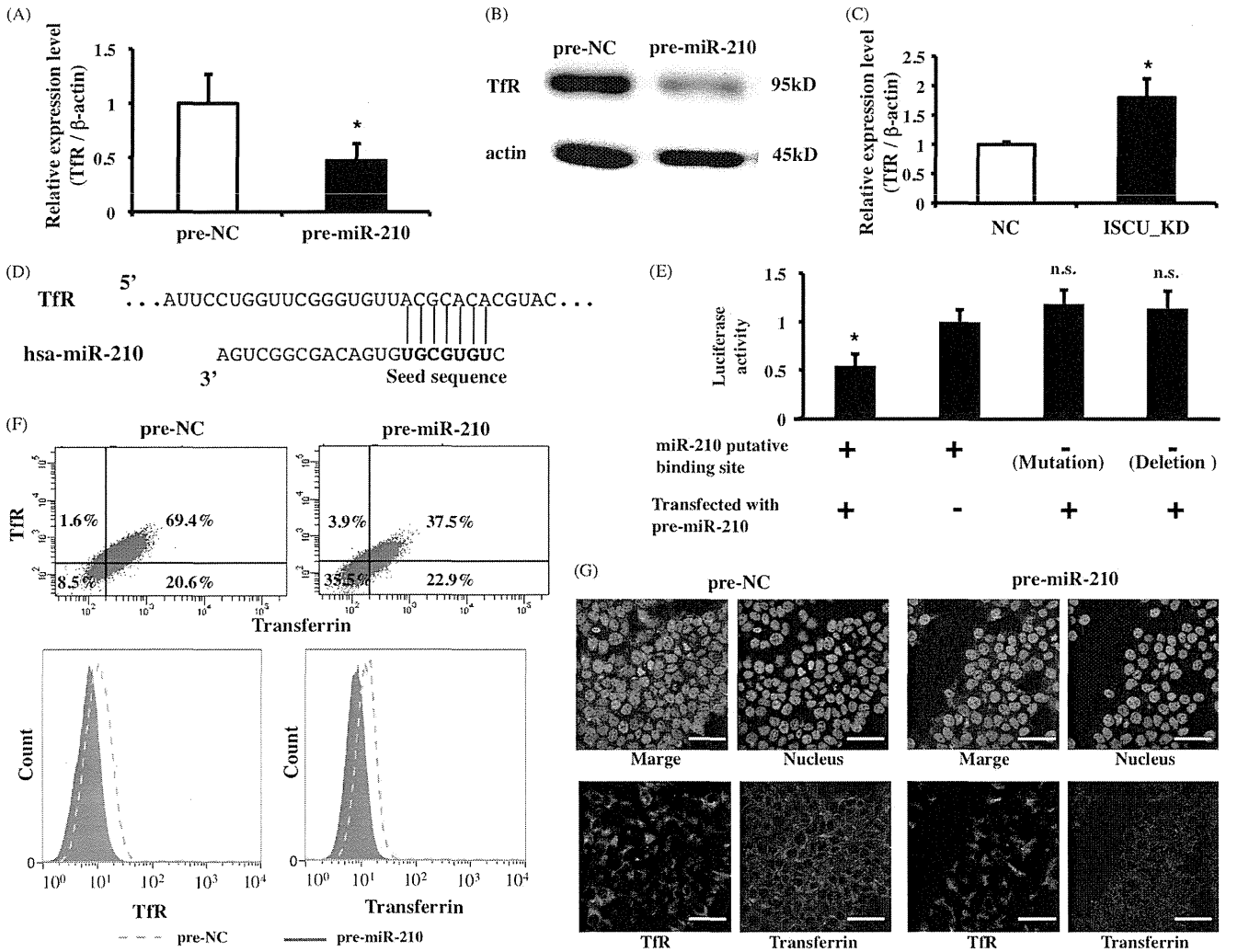

FIGURE 2. **miR-210 also represses the expression of TfR as a target gene.** *A*, MCF7 cells were transfected with pre-miR-210 or pre-NC. After 48 h, TfR expression was detected by qRT-PCR. β-Actin was used as a control. *, $p < 0.05$ compared with pre-NC. *B*, MCF7 cells were transfected with pre-miR-210 or pre-NC. After 48 h, TfR expression was detected by immunoblotting. Actin was used as a loading control. *C*, expression of TfR is increased by knockdown of ISCU. TfR expression was detected in ISCU knockdown cells by qRT-PCR. β-Actin was used as a control. *ISCU_KD*, ISCU knockdown cell line; *NC*, control cell line. *, $p < 0.05$ compared with the control group. *D*, the predicted binding site for miR-210 at 3′-UTR of TfR gene is shown. The *bold font* shows the seed sequence of miR-210. *E*, MCF7 cells were co-transfected with pre-miR-210 or pre-NC and psi-TfR or with its mutant or deletion vector. After 48 h, luciferase activities were measured. *, $p < 0.05$ compared with pre-NC. *n.s.*, not significant. *F*, MCF7 cells were transfected with pre-miR-210 or pre-NC. After 48 h, transfected cells were incubated with Alexa Fluor 594-labeled Tf for 45 min. Expression of TfR (*y* axis) and uptake of transferrin (*x* axis) (*upper panel*) were analyzed by FACS. The *right lower panel* represents the expression of TfR. The *left lower panel* represents uptake of transferrin. *Dashed histogram*, transfected pre-NC; *filled histogram*, transfected pre-miR-210. *G*, MCF7 cells were transfected with pre-miR-210 or pre-NC. After 48 h, transfected cells were incubated with Alexa Fluor 594-labeled Tf (*red*) for 45 min and fixed in 4% paraformaldehyde for 30 min. Subsequently, cells were immunostained using anti-TfR antibody and an Alexa Fluor 488-conjugated secondary antibody (*green*). The nucleus was then stained with the Hoechst 33342 (*blue*). *Scale bar*, 50 μm.

cancer cells. These results prompted us with the idea that iron-ISCU pathway might regulate the iron homeostasis in breast cancer cells.

miR-210 Suppresses the Major Iron-uptake Protein TfR—In mammalian cells, knockdown of ISCU markedly reduces mitochondrial aconitase activity and then promotes the activity of IRP1. Activation of IRP1 accelerates the binding to multiple iron-responsive elements in the 3′-UTR of the mRNA, such as TfR involved in iron acquisition, then leading to increased mRNA stability (26). When IRP1 binds to the 3′-UTR of TfR mRNA, which is an iron-uptake protein, the transcript is protected from degradation. Therefore, we hypothesized that overexpression of miR-210 stabilizes mRNA of TfR via the activation of IRP1. To prove this hypothesis, we measured the expression of mRNA and the protein level of TfR after transfection of the miR-210 mimic (pre-miR-210) in MCF7 and MM231 cells. Surprisingly, the expression of TfR was down-regulated after the transfection of pre-miR-210 (Fig. 2, *A* and *B*, and supplemental Fig. S4*A*). This is an unexpected result because the expression of TfR was increased in ISCU stably knockdown cells (Fig. 2*C* and supplemental Fig. S2*E*). Those results led us to consider that miR-210 directly suppressed the expression of TfR by binding to the 3′-UTR of TfR. To check whether or not TfR is a direct target gene of miR-210, we once again used *in silico* algorithms and found that there was an miR-210-binding site at 3′-UTR of TfR (Fig. 2*D*). To prove that miR-210 directly recognizes the identical predicted target site in the 3′-UTR of TfR, MCF7 cells were transfected with psi-TfR, which was fused to 3′-UTR of TfR and the luciferase open reading frame, or a control vector. In addition, we also prepared

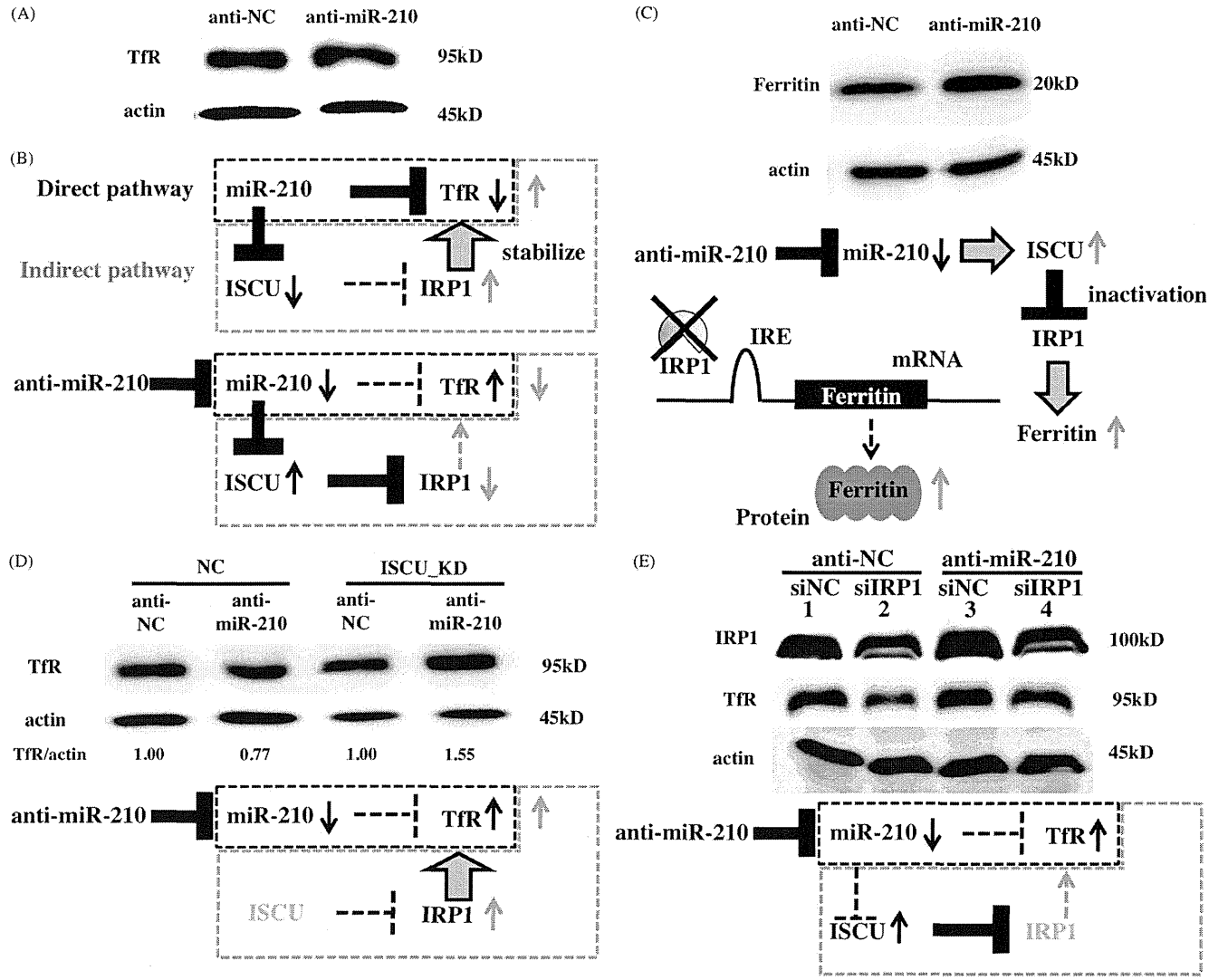

FIGURE 3. **miR-210 has two pathways for regulating TfR expression.** *A*, MCF7 cells were transfected with anti-miR-210 or anti-NC and exposed to 1% O_2 for 48 h. TfR expression was detected by immunoblotting. Actin was used as a loading control. *B*, schematic represents the regulation of two miR-210 target genes after treatment with anti-miR-210. After the transfection of anti-miR-210, the expression of TfR was indirectly decreased via the up-regulation of ISCU. On the other hand, the expression of TfR was directly increased through the down-regulation of miR-210. The expression of TfR then seemed to be unchanged after the transfection of anti-miR-210. *Direct pathway* means that miR-210 recognized the 3′-UTR of TfR and directly (see *black box*) regulates its expression. On the other hand, *Indirect pathway* means that miR-210 indirectly regulates TfR expression through the ISCU-IRP1 pathway (see *gray box*). After the transfection of anti-miR-210 (see *lower panel*), the expression of miR-210 was down-regulated, and then the expression of TfR was up-regulated (see *black box*). On the other hand, expression of ISCU was up-regulated after the transfection of anti-miR-210, and then the activity of IRP1 was inhibited by up-regulation of ISCU. IRP1 was important for the translation of TfR. Thus, inhibition of IRP1 activity by up-regulation of ISCU results in the down-regulation of TfR (see *gray box*). *C*, MCF7 cells were transfected with anti-miR-210 or anti-NC and exposed to 1% O_2. After 48 h, ferritin expression was detected by immunoblotting. Actin was used as a loading control. *Lower panel* shows schematic representation of the regulation of miR-210 target gene and ferritin after treatment with anti-miR-210. *D*, ISCU knockdown cell lines were transfected with anti-miR-210 or anti-NC and exposed to 1% O_2 for 48 h. TfR expression was detected by immunoblotting and quantified by densitometry. Actin was used as a loading control. *Lower panel* shows schematic representation of the regulation of miR-210 target gene after treatment with anti-miR-210 in *ISCU_KD* cells. Because ISCU was stably suppressed by shRNA in these cells, the activity of IRP1 was increased (*gray box*). Therefore, in this experiment, TfR was up-regulated by not only the down-regulation of miR-210 that directly targets the TfR but also the activation by IRP1. *E*, MCF7 cells were transfected with anti-miR-210 or anti-NC and siIRP1 or siNC and exposed to 1% O_2 for 48 h. Expression of IRP1 (*upper*) and TfR (*middle*) was detected by immunoblotting. Actin was used as a loading control. *Lower panel* shows schematic representation of the regulation of miR-210 target gene after treatment with anti-miR-210 and siIRP1. Because the expression of IRP1 was suppressed by siRNA, there is no influence on the TfR expression by *Indirect pathway* (*gray box*). On the other hand, the expression of miR-210 was down-regulated by anti-miR-210. As a result, TfR was up-regulated in this experiment.

psi-TfR_mut, which has a mutated sequence of a putative miR-210-binding site or psi-TfR_del, which has deleted a putative miR-210-binding site. Co-transfection of pre-miR-210 down-regulated *Renilla* luciferase activity significantly more than in pre-NC in the presence of psi-TfR. In contrast, *Renilla* luciferase activity was not altered in the presence of psi-TfR_del or psi-TfR_mut (Fig. 2*E*). We confirmed that miR-210 targets the 3′-UTR of TfR mRNA, showing that miR-210 directly suppresses not only ISCU but also TfR. TfR plays a major role in cellular iron uptake through binding to and internalizing a carrier protein transferrin (Tf). Therefore, to examine whether reduction of TfR by transfected pre-miR-210 functionally inhibited the uptake of Tf or not, Alexa Fluor 594-labeled Tf was used to monitor the uptake of Tf by immunostaining and FACS analysis. As shown in Fig. 2, *F* and *G*, uptake of Tf was lower in pre-miR-210-transfected cells than in control cells,

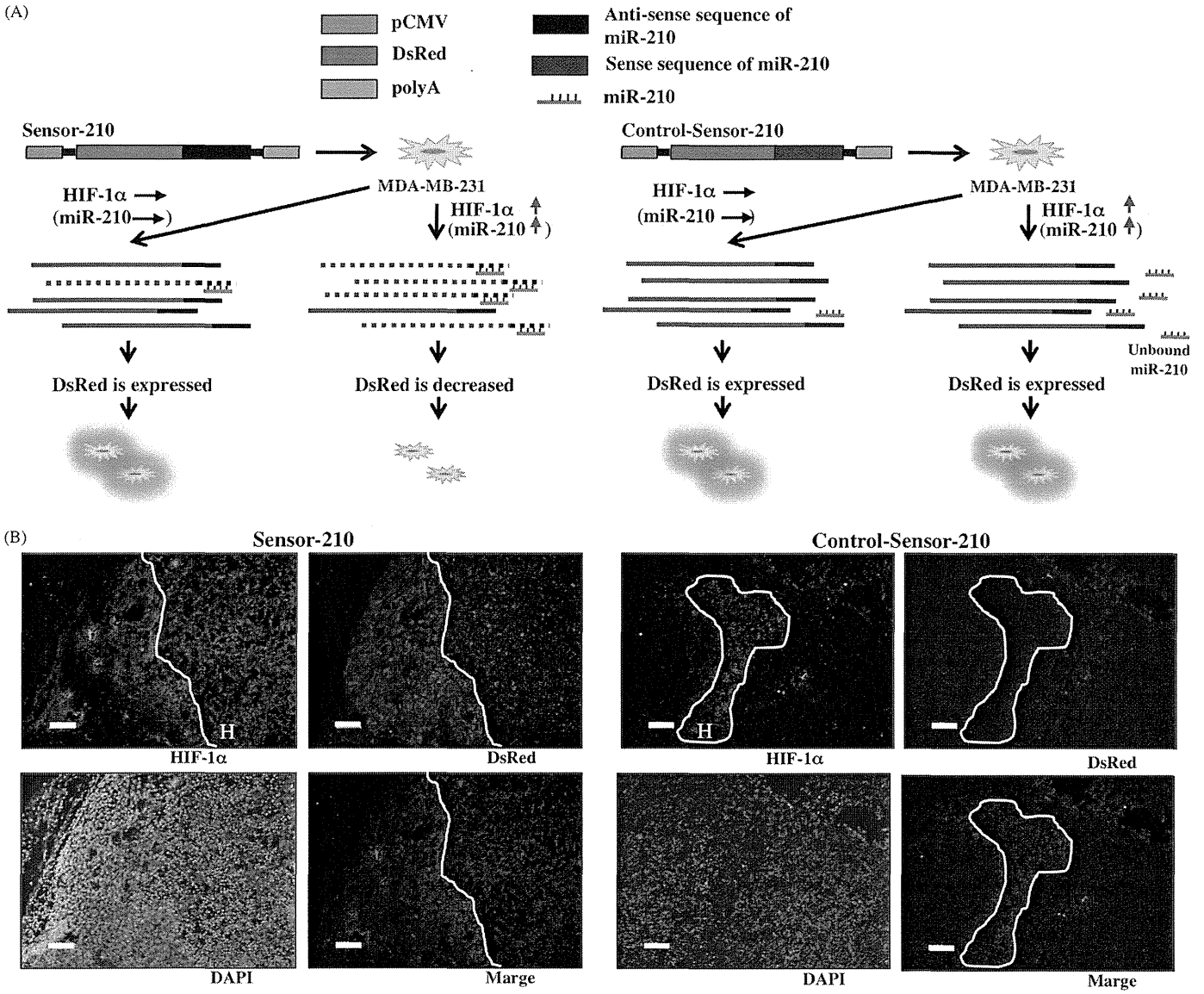

FIGURE 4. **miR-210-expressing cells were localized in the chronic hypoxic region of inoculated tumor cells.** *A*, schematic represents miR-210 tracing assay. In the hypoxic condition, expression of miR-210 is increased by the HIF-1, and then the transcripts of DsRed are degraded by miR-210 (*dashed lines with red and black*). On the other hand, expression of miR-210 is not changed under the normoxic condition (*lines with red and black*). In addition, the fluorescence of Control-Sensor-210 was not changed even under hypoxic conditions. Because their miR-210-binding sites were inserted inversely, the miR-210 could not bind to the 3′-UTR of DsRed. *B*, immunohistochemical analysis of DsRed in the tumor is shown. Sections were stained with the rabbit polyclonal anti-red fluorescent protein antibody and the mouse monoclonal anti-HIF-1α antibody. The fluorescence of DsRed could not be observed in HIF-1α-positive regions in the Sensor-210-inoculated tumor; on the other hand, there was uniform fluorescence of DsRed in Control-Sensor-210-cells-inoculated tumor. *H*, hypoxic region in a tumor is indicated. *Scale bar*, 100 μm.

indicating a direct correlation between TfR reduction and the decreased uptake of Tf in miR-210-overexpressing cells (Fig. 2, *F* and *G*). We also confirmed similar results using an MM231 cells (supplemental Fig. S4, *B* and *C*). Consequently, these observations indicated that overexpression of miR-210 decreases the concentration of intracellular iron by inhibiting the Tf-TfR-dependent iron-uptake system.

miR-210 Is a Member of Iron Homeostatic Networks—As shown in Fig. 2, overexpression of miR-210 inhibited the uptake of Tf via the suppression of TfR. However, because overexpression of miR-210 by miR-210 mimics transduces an extremely high amount of miRNA in the cells (supplemental Fig. S3*A*), it is necessary to examine the function of miR-210 in iron homeostasis under physiological conditions. To evaluate the physiological relationship among miR-210, ISCU, and TfR expression, we transfected antisense miR-210 oligonucleotide (anti-miR-210), which suppresses the expression of miR-210 (supplemental Fig. S3*B*) and control oligonucleotide (anti-NC) into MCF7 cells under a hypoxic condition. We observed the induction of ISCU expression level after the transfection of anti-miR-210 (Fig. 1*F* and supplemental Fig. S2*D*); however, the expression of TfR was not affected (Fig. 3*A* and supplemental Fig. S5*A*). The knockdown of ISCU has been known to increase the expression of TfR by activating IRP1 activity (Fig. 2*C*) (26). From these observations, we assumed that unchanged TfR expression after the transfection of anti-miR-210 was caused by the up-regulation of the ISCU expression level by anti-miR-210 (Fig. 3*B*), leading to the inhibition of IRP1 activity without affecting the

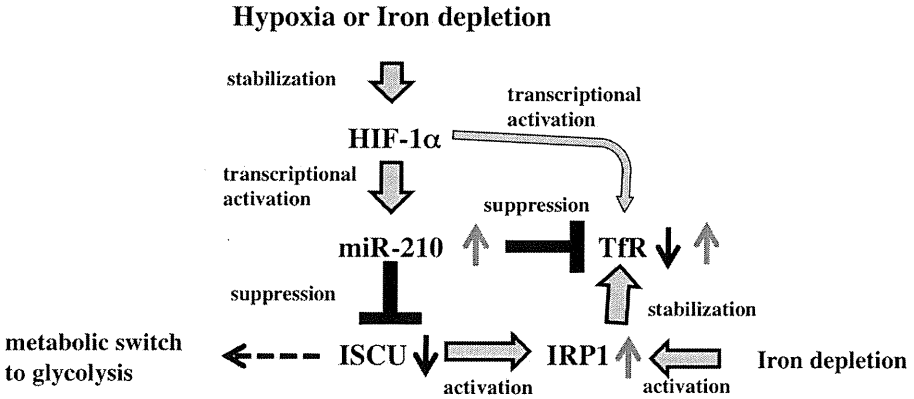

FIGURE 5. **Schematic representation of our proposed model.** miR-210 is induced by hypoxia and iron depletion and directly suppresses two iron homeostasis-related proteins. miR-210 regulates the iron homeostasis with dual pathways of regulating TfR expression. The *gray arrows* indicate up-regulation, and the *black arrows* indicate down-regulation. The *dashed arrow* indicates shift to metabolic switch.

IRP1 expression level. To confirm the change of IRP1 activity by miR-210 expression level in our experiment, we transfected anti-miR-210 or pre-miR-210 into MCF7 cells and analyzed the expression level of ferritin protein, which is the iron storage protein, by immunoblotting. Because the 5′-UTR of ferritin mRNA contains a single iron-responsive element that affects translation initiation, inhibition of IRP1 activity led to the up-regulation of ferritin expression (29). Indeed, the expression level of ferritin was increased in anti-miR-210-transfected cells compared with that in anti-NC-transfected cells (Fig. 3*C*). On the other hand, overexpression of miR-210 by pre-miR-210 suppressed the expression of ferritin in MCF7 cells, indicating that the activity of IRP1 was modulated by miR-210 through ISCU pathway (supplemental Fig. S5*B*). To eliminate the effect of ISCU on TfR expression in this assay system, we established stable ISCU knockdown cell lines using the MCF7 cell. In ISCU knockdown cells, the expression of TfR was higher than that in control cells by activated IRP1 (Fig. 2*C* and supplemental Fig. S2*E*). We carried out the same experiment as shown in Fig. 3*A* using ISCU knockdown cell lines and observed that anti-miR-210 increased TfR mRNA and protein level in ISCU knockdown cell lines but not in control cell lines (Fig. 3*D*). This result indicated that the expression of TfR was up-regulated by not only the down-regulation of miR-210 that directly target the TfR but also the activated IRP1, which is usually inactivated by ISCU. Furthermore, MCF7 cells were transfected with siRNA against IRP1 (or siNC) and anti-miR-210 (or anti-NC) under hypoxic condition, and these cells were analyzed for the expression of IRP1 and TfR by immunoblotting. As a result, because the IRP1 is known to stabilize the TfR mRNA, knockdown of IRP1 by siRNA caused a decrease in the expression of TfR (Fig. 3*E*; compare *lanes 1* and *2*). Importantly, co-transfection of anti-miR-210 and IRP1 siRNA induced the expression of TfR, indicating that miR-210 directly targets the TfR in cancer cells (Fig. 3*E*; compare *lanes 2* and *4*). Taken together, these data suggest that miR-210 regulates TfR expression through direct and indirect translational regulatory mechanisms to fine-tune the iron homeostasis (Fig. 3*B*).

The Distribution of miR-210-expressing Cells Is Associated with Chronic Hypoxia—Most tumors have lower median O_2 partial pressures than their tissue of origin and are deprived of nutrients, including iron (30). Significant variations in these relevant parameters must be expected between different locations within the same tumor at the same location at different times and between individual tumors of the same grading and staging. Previous results have shown that the expression of miR-210 is modulated by the cellular iron concentration and oxygen tension; however, what kinds of cells *in vivo* expressed miR-210 have not been clarified yet. For this reason, we postulated that clarifying the distribution of miR-210-expressing cells in the tumor leads to the understanding of cancer metabolism regulated by iron concentration. To answer this, we investigated the distribution of miR-210-expressing cells in an *in vivo* breast tumor xenograft model. In this experiment, we prepared the cell line, called MDA-MB-231-miR-210-sensor, to trace the expression of miRNA-210 *in vivo*. Because this cell was established by DsRed harboring a complementary sequence of miR-210, the fluorescence of DsRed was diminished when the expression of miR-210 was induced (Fig. 4*A* and supplemental Fig. S6*A*). We injected 5×10^6 MDA-MB-231-miR-210-sensor cells into nude mice. Prior to the excision of tumors, the mice were administered pimonidazole, a compound that binds irreversibly to hypoxic cells (31). Serial sections of the tumors were subsequently stained for pimonidazole, HIF-1α, and DsRed. A correlation between HIF-1α-positive cells and DsRed-negative cells, indicative of diminishment of DsRed expression by miR-210, was observed at the hypoxic rim around necrotic regions of the tumor, a location typically associated with chronic hypoxia (Fig. 4*B*). We also observed that pimonidazole-positive cells and DsRed-negative cells overlapped. On the other hand, fluorescence of control-miR-210-sensor cells, whose miR-210-binding site was inserted inversely with the miR-210-sensor vector, was not changed in inoculated tumor cells. Furthermore, we also established a cell line that enabled us to trace the expression of miR-210 by its promoter-driven DsRed (Fig. S6*B*) and obtained similar results with the MDA-MB-231-miR-210-sensor (Fig. S6*C*). Together, these observations indicated that the expression of miR-210 was

increased in the severely hypoxic region of the tumor. Namely, miR-210 regulates the iron homeostasis in cancer cells under the chronic hypoxic condition in tumors.

DISCUSSION

Iron is indispensable for the function of many prosthetic groups, whereas excess free iron can oxidize and damage the protein, nucleic acid, and lipid contents of cells. Thus, animals evolved complex mechanisms to control the favorable concentrations of intracellular iron. In this study, we revealed that miR-210 is involved in a novel iron homeostasis mechanism through the association of ISCU and TfR in cancer cells (Fig. 5). miR-210 down-regulates ISCU and the Fe-S cluster to mediate the energy metabolic shift from aerobic oxidative phosphorylation to anaerobic glycolysis (32). Concurrently, reduction of the Fe-S cluster activates IRP1, and, subsequently, the expression of TfR is increased, resulting in the elevated uptake of the iron ion. However, several reports show that the excess iron can be toxic (4). To reduce the cellular iron concentration, miR-210 directly suppresses the expression of TfR. Thus, miR-210 regulates iron homeostasis and avoids intracellular iron toxicity.

Compared with normal cells, cancer cells require a large amount of iron; thus, they generally proliferate at a larger rate than their normal counterparts. Hence, iron chelators exert their anti-proliferative effects on tumors (12). Moreover, a previous report showed that down-regulation of TfR decreased cellular proliferation and altered expression of genes involved in cell cycle control (33). Thus, as summarized in Fig. 5, it is postulated that miR-210 has two pathways for the regulation of TfR expression. One is the TfR up-regulation pathway via suppression of ISCU (indirect pathway), and the other one is the TfR down-regulation pathway by direct binding to TfR mRNA. Reduction of ISCU only increases the binding activity of IRP1, but its level of expression does not change. Thus, the effect of up-regulation of TfR by reduced ISCU depends on the amount of IRP1 protein. There are limitations to the up-regulation of TfR by the indirect pathway. Then, in the case of a further increase of miR-210, direct suppression of TfR is superior to its up-regulation by the indirect pathway. In other words, because the forced expression of miR-210 overwhelms the indirect pathway, the direct pathway is superior to the indirect one. Therefore, exogenous transfection of miR-210 causes TfR suppression (Fig. 2), thereby reducing cellular proliferation (supplemental Fig. S7) (34, 35). Moreover, we confirmed the overlap of chronic hypoxic regions and miR-210-expressing cells in inoculated cancer cells *in vivo*. These observations suggest that precise regulation of miR-210 expression level is vital for maintaining the iron homeostasis, leading to the survival and proper cellular proliferation of cancer cells.

HIFs and IRPs are key mediators of cellular iron homeostasis and oxygen, respectively. Because iron and oxygen are often intimately connected in their metabolism, it is not surprising that their levels are coordinately regulated in cells. Such cross-talk is achieved in part by cellular regulatory factors that sense and respond to both iron and oxygen, and it is reinforced by the overlap in the gene targets regulated by each pathway. For instance, binding of IRPs protects TfR mRNA from degradation, and HIF-1α activates TfR gene transcription (36, 37). In addition, in this study, we identified that hypoxia-inducible miR-210 was a key component of this pathway.

As noted above, we have clearly shown that iron homeostasis is micromanaged by miRNAs. Therefore, miRNAs could be essential for maintaining other metal homeostasis in mammals; for example, copper, zinc, and cadmium. In agreement with our observations, the current view on the molecular understanding of miRNA-guided regulation of plant heavy metal adaption was reported (38, 39). Dysregulation of metal homeostasis-related miRNAs may contribute to various diseases including cancers, nephropathy, and autoimmune disease. Further analyses are required on how these miRNAs can be affected by genetic and epigenetic mechanisms in the physiological and pathological microenvironments.

Acknowledgments—We thank Haruhisa Iguchi and Ryou-u Takahashi for participation in discussions and technical advice, Yusuke Yamamoto for participation in helpful discussions, Ayako Inoue, and Keitaro Hagiwara for excellent technical assistance.

REFERENCES

1. Que, L., Jr., and Ho, R. Y. (1996) Dioxygen activation by enzymes with mononuclear nonheme iron active sites. *Chem. Rev.* **96,** 2607–2624
2. Pau, M. Y., Lipscomb, J. D., and Solomon, E. I. (2007) Substrate activation for O_2 reactions by oxidized metal centers in biology. *Proc. Natl. Acad. Sci. U.S.A.* **104,** 18355–18362
3. Hegg, E. L., and Que, L., Jr. (1997) The 2-His-1-carboxylate facial triad: an emerging structural motif in mononuclear nonheme iron(II) enzymes. *Eur. J. Biochem.* **250,** 625–629
4. Stadtman, E. R. (1990) Metal ion-catalyzed oxidation of proteins: biochemical mechanism and biological consequences. *Free Radic. Biol. Med.* **9,** 315–325
5. Clark, S. F. (2009) Iron-deficiency anemia: diagnosis and management. *Curr. Opin. Gastroenterol.* **25,** 122–128
6. Raja, K. B., Duane, P., and Peters, T. J. (1990) Effects of turpentine-induced inflammation on the hypoxic stimulation of intestinal Fe^{3+} absorption in mice. *Int. J. Exp. Pathol.* **71,** 785–789
7. Laftah, A. H., Raja, K. B., Latunde-Dada, G. O., Vergi, T., McKie, A. T., Simpson, R. J., and Peters, T. J. (2005) Effect of altered iron metabolism on markers of haem biosynthesis and intestinal iron absorption in mice. *Ann. Hematol.* **84,** 177–182
8. Peyssonnaux, C., Zinkernagel, A. S., Schuepbach, R. A., Rankin, E., Vaulont, S., Haase, V. H., Nizet, V., and Johnson, R. S. (2007) Regulation of iron homeostasis by the hypoxia-inducible transcription factors (HIFs). *J. Clin. Invest.* **117,** 1926–1932
9. Wang, G. L., Jiang, B. H., Rue, E. A., and Semenza, G. L. (1995) Hypoxia-inducible factor 1 is a basic-helix-loop-helix-PAS heterodimer regulated by cellular O_2 tension. *Proc. Natl. Acad. Sci. U.S.A.* **92,** 5510–5514
10. Wang, G. L., and Semenza, G. L. (1995) Purification and characterization of hypoxia-inducible factor 1. *J. Biol. Chem.* **270,** 1230–1237
11. Campbell, J. A. (1940) Effects of precipitated silica and of iron oxide on the incidence of primary lung tumors in mice. *Br. Med. J.* **2,** 275–280
12. Richardson, D. R., Kalinowski, D. S., Lau, S., Jansson, P. J., and Lovejoy, D. B. (2009) Cancer cell iron metabolism and the development of potent iron chelators as anti-tumor agents. *Biochim. Biophys. Acta* **1790,** 702–717
13. Bartel, D. P. (2004) MicroRNAs: genomics, biogenesis, mechanism, and function. *Cell* **116,** 281–297
14. Stefani, G., and Slack, F. J. (2008) Small noncoding RNAs in animal development. *Nat. Rev. Mol. Cell Biol.* **9,** 219–230
15. Calin, G. A., and Croce, C. M. (2006) MicroRNA signatures in human cancers. *Nat. Rev. Cancer* **6,** 857–866
16. Rasmussen, K. D., Simmini, S., Abreu-Goodger, C., Bartonicek, N., Di Giacomo, M., Bilbao-Cortes, D., Horos, R., Von Lindern, M., Enright, A. J.,

and O'Carroll, D. (2010) The miR-144/451 locus is required for erythroid homeostasis. *J. Exp. Med.* **207,** 1351–1358
17. Kosaka, N., Sugiura, K., Yamamoto, Y., Yoshioka, Y., Miyazaki, H., Komatsu, N., Ochiya, T., and Kato, T. (2008) Identification of erythropoietin-induced microRNAs in haematopoietic cells during erythroid differentiation. *Br. J. Haematol.* **142,** 293–300
18. Camps, C., Buffa, F. M., Colella, S., Moore, J., Sotiriou, C., Sheldon, H., Harris, A. L., Gleadle, J. M., and Ragoussis, J. (2008) HSA-miR-210 is induced by hypoxia and is an independent prognostic factor in breast cancer. *Clin. Cancer Res.* **14,** 1340–1348
19. Friedman, R. C., Farh, K. K., Burge, C. B., and Bartel, D. P. (2009) Most mammalian mRNAs are conserved targets of microRNAs. *Genome Res.* **19,** 92–105
20. Griffiths-Jones, S., Grocock, R. J., van Dongen, S., Bateman, A., and Enright, A. J. (2006) miRBase: microRNA sequences, targets, and gene nomenclature. *Nucleic Acids Res.* **34,** D140–144
21. Wang, X., and El Naqa, I. M. (2008) Prediction of both conserved and nonconserved microRNA targets in animals. *Bioinformatics* **24,** 325–332
22. Huang, X., Ding, L., Bennewith, K. L., Tong, R. T., Welford, S. M., Ang, K. K., Story, M., Le, Q. T., and Giaccia, A. J. (2009) Hypoxia-inducible miR-210 regulates normoxic gene expression involved in tumor initiation. *Mol. Cell* **35,** 856–867
23. Fujita, S., Ito, T., Mizutani, T., Minoguchi, S., Yamamichi, N., Sakurai, K., and Iba, H. (2008) miR-21 gene expression triggered by AP-1 is sustained through a double-negative feedback mechanism. *J. Mol. Biol.* **378,** 492–504
24. Burk, U., Schubert, J., Wellner, U., Schmalhofer, O., Vincan, E., Spaderna, S., and Brabletz, T. (2008) A reciprocal repression between ZEB1 and members of the miR-200 family promotes EMT and invasion in cancer cells. *EMBO Rep.* **9,** 582–589
25. Ye, H., and Rouault, T. A. (2010) Erythropoiesis and iron-sulfur cluster biogenesis. *Adv. Hematol.* **2010,** 10.1155/2010/329394
26. Tong, W. H., and Rouault, T. A. (2006) Functions of mitochondrial ISCU and cytosolic ISCU in mammalian iron-sulfur cluster biogenesis and iron homeostasis. *Cell Metab.* **3,** 199–210
27. Chen, Z., Li, Y., Zhang, H., Huang, P., and Luthra, R. (2010) Hypoxia-regulated microRNA-210 modulates mitochondrial function and decreases ISCU and COX10 expression. *Oncogene* **29,** 4362–4368
28. Favaro, E., Ramachandran, A., McCormick, R., Gee, H., Blancher, C., Crosby, M., Devlin, C., Blick, C., Buffa, F., Li, J. L., Vojnovic, B., Pires das Neves, R., Glazer, P., Iborra, F., Ivan, M., Ragoussis, J., and Harris, A. L. (2010) MicroRNA-210 regulates mitochondrial free radical response to hypoxia and Krebs cycle in cancer cells by targeting iron-sulfur cluster protein ISCU. *PLoS One* **5,** e10345
29. Hentze, M. W., Caughman, S. W., Rouault, T. A., Barriocanal, J. G., Dancis, A., Harford, J. B., and Klausner, R. D. (1987) Identification of the iron-responsive element for the translational regulation of human ferritin mRNA. *Science* **238,** 1570–1573
30. Vaupel, P., Kallinowski, F., and Okunieff, P. (1989) Blood flow, oxygen and nutrient supply, and metabolic microenvironment of human tumors: a review. *Cancer Res.* **49,** 6449–6465
31. Raleigh, J. A., Chou, S. C., Arteel, G. E., and Horsman, M. R. (1999) Comparisons among pimonidazole binding, oxygen electrode measurements, and radiation response in C3H mouse tumors. *Radiat. Res.* **151,** 580–589
32. Chan, S. Y., Zhang, Y. Y., Hemann, C., Mahoney, C. E., Zweier, J. L., and Loscalzo, J. (2009) MicroRNA-210 controls mitochondrial metabolism during hypoxia by repressing the iron-sulfur cluster assembly proteins ISCU1/2. *Cell Metab.* **10,** 273–284
33. O'Donnell, K. A., Yu, D., Zeller, K. I., Kim, J. W., Racke, F., Thomas-Tikhonenko, A., and Dang, C. V. (2006) Activation of transferrin receptor 1 by c-Myc enhances cellular proliferation and tumorigenesis. *Mol. Cell. Biol.* **26,** 2373–2386
34. Chitambar, C. R., Massey, E. J., and Seligman, P. A. (1983) Regulation of transferrin receptor expression on human leukemic cells during proliferation and induction of differentiation: effects of gallium and dimethylsulfoxide. *J. Clin. Invest.* **72,** 1314–1325
35. Neckers, L. M., and Trepel, J. B. (1986) Transferrin receptor expression and the control of cell growth. *Cancer Invest.* **4,** 461–470
36. Lok, C. N., and Ponka, P. (1999) Identification of a hypoxia-response element in the transferrin receptor gene. *J. Biol. Chem.* **274,** 24147–24152
37. Tacchini, L., Bianchi, L., Bernelli-Zazzera, A., and Cairo, G. (1999) Transferrin receptor induction by hypoxia: HIF-1-mediated transcriptional activation and cell-specific post-transcriptional regulation. *J. Biol. Chem.* **274,** 24142–24146
38. Yamasaki, H., Abdel-Ghany, S. E., Cohu, C. M., Kobayashi, Y., Shikanai, T., and Pilon, M. (2007) Regulation of copper homeostasis by microRNA in *Arabidopsis*. *J. Biol. Chem.* **282,** 16369–16378
39. Abdel-Ghany, S. E., and Pilon, M. (2008) MicroRNA-mediated systemic down-regulation of copper protein expression in response to low copper availability in *Arabidopsis*. *J. Biol. Chem.* **283,** 15932–15945

SCIENTIFIC REPORTS

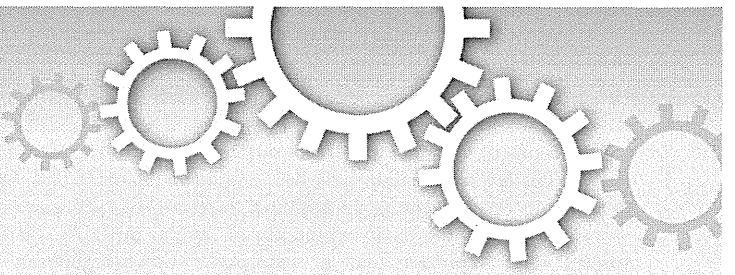

OPEN

SUBJECT AREAS:
NON-CONDING RNA'S
RNAI
SMALL RNA'S
TUMOUR SUPPRESSORS

Received
1 December 2011

Accepted
24 February 2012

Published
15 March 2012

Correspondence and requests for materials should be addressed to T.O. (tochiya@ncc.go.jp)

Stilbene derivatives promote Ago2-dependent tumour-suppressive microRNA activity

Keitaro Hagiwara[1,2], Nobuyoshi Kosaka[1], Yusuke Yoshioka[1], Ryou-u Takahashi[1], Fumitaka Takeshita[1] & Takahiro Ochiya[1,2]

[1]Division of Molecular and Cellular Medicine, National Cancer Center Research Institute, 5-1-1, Tsukiji, Chuo-ku, Tokyo 104-0045, Japan, [2]Department of Biological Sciences, Tokyo Institute of Technology, 4259 Nagatsuta-cho, Midori-ku, Yokohama 226-8501, Japan.

It is well known that natural products are a rich source of compounds for applications in medicine, pharmacy, and biology. However, the exact molecular mechanisms of natural agents in human health have not been clearly defined. Here, we demonstrate for the first time that the polyphenolic phytoalexin resveratrol promotes expression and activity of Argonaute2 (Ago2), a central RNA interference (RNAi) component, which thereby inhibits breast cancer stem-like cell characteristics by increasing the expression of a number of tumour-suppressive miRNAs, including miR-16, -141, -143, and -200c. Most importantly, resveratrol-induced Ago2 resulted in a long-term gene silencing response. We also found that pterostilbene, which is a natural dimethylated resveratrol analogue, is capable of mediating Ago2-dependent anti-cancer activity in a manner mechanistically similar to that of resveratrol. These findings suggest that the dietary intake of natural products contributes to the prevention and treatment of diseases by regulating the RNAi pathway.

Natural products are a rich source of valuable medicinal agents. More than half of the currently available drugs are natural or related compounds. In the case of cancer, the percentage of natural compounds exceeds 60%. Research on natural products as potential anti-cancer agents dates back to at least the Egyptian Ebers Papyrus of 1550 B.C. However, more recent scientific investigations began with the studies of Hartwell and co-workers on the application of podophyllotoxin and its derivatives as anti-cancer agents[1]. A large number of plant, marine, and microbial sources have been tested, and hundreds of active compounds have been isolated. Despite these advances, the underlying mechanisms of natural products in human health are not fully understood.

Resveratrol, which is a multi-functional polyphenolic compound, is a phytoalexin present in a wide variety of plant species, including grapes, mulberries, and peanuts[2]. Since its discovery, resveratrol has been shown to exhibit a plethora of physiological properties that may be useful in human medicine. More interest was focused on resveratrol at the beginning of the 1990s when it was first shown to be present in red wine[3]. Experimental studies have shown that resveratrol inhibits the growth of various cancer cells and induces apoptotic cell death[4,5]. Recently, a phase I/II clinical trial in patients with colon cancer was conducted to examine the effects of resveratrol treatment on colon cancer progression and colonic mucosa in patients with colon cancer and its effects in modulating the Wnt signalling pathway[2]. Although these data provide evidence of multiple anti-tumour effects induced by resveratrol, the exact mechanism is not clearly understood.

MicroRNAs (miRNAs) have emerged as key post-transcriptional regulators of gene expression that are involved in diverse physiological and pathological processes[6]. The inhibition of the miRNA biogenesis pathway results in severe developmental defects and lethality in many organisms[7]. It has been suggested that a considerable number of miRNAs have roles in cancer cells. Indeed, an increasing number of experimental studies have shown that the knock-down or the re-expression of specific miRNAs could induce drug sensitivity, inhibit the proliferation of cancer cells, and suppress cancer cell invasion and metastasis[8–10]. Recent studies have shown that natural products, including curcumin, isoflavone, I3C, DIM, and EGCG, could alter the expression of specific miRNAs, which may lead to the increased sensitivity of cancer cells to conventional anti-cancer agents and, therefore, tumour growth inhibition[11–14]. However, the exact molecular mechanism of miRNA induction and the biological significance of resveratrol-induced miRNAs have not been reported.

Diet is one of the most important modifiable cancer risk determinants[15]. Dietary components have been implicated in many pathways involved in carcinogenesis. In addition, carcinogenic processes are associated with the altered expression of several miRNAs. Recent studies have reported that a widespread down-regulation of miRNAs is commonly observed during human cancer-cell initiation and progression[16,17]. In this study, we hypothesised that the dietary intake of natural products maintains tumour-suppressive miRNA expression in cancer cells, leading to the prevention of carcinogenesis. We demonstrated that resveratrol suppresses cancer cell malignancy *in vitro* and *in vivo* through the transcriptional activation of tumour-suppressive miRNAs and Argonaute2 (Ago2). Furthermore, we provided evidence that Ago2 over-expression enhances the RNA interference (RNAi) activity. These findings suggest that the dietary intake of natural products safely reduces a wide range of negative consequences with an overall improvement in human health and survival by modulating miRNA biogenesis.

Results

Resveratrol reduces the cancer stem-like cells population by up-regulating miR-141 and miR-200c. To identify the potential anti-cancer activity of resveratrol, we investigated the effects of this compound on tumour formation *in vivo*. We orthotopically inoculated female SCID hairless outbred mice with MDA-MB-231-luc-D3H2LN cells (200 cells), which were then treated with resveratrol (25 mg/kg/day) or ethanol (control) via intraperitoneal injection every day for one week. Tumour growth was then monitored using an IVIS imaging system. The weight of the mice did not significantly change between the groups during the course of the experiment, suggesting that resveratrol did not have notable adverse effects on mice (Supplementary Fig. 1a). The results demonstrated that the resveratrol administration into the mice significantly suppressed tumour formation, while obvious tumours were observed in vehicle-treated mice, indicating that resveratrol is capable of inhibiting the survival and growth of cancer cells *in vivo* (Fig. 1a). A recent report has shown that solid tumours contain a distinct population of cells with the ability to form tumours in mice; these cells are known as tumour-initiating or cancer stem-like cells (CSCs) and display increased drug resistance and metastatic ability because they consistently form tumours, whereas other cancer cell populations were depleted of cells capable of tumour formation[18,19]. To identify the effects of resveratrol on the CSC phenotype, breast cancer cells were examined for changes in the CSC population, which is a highly tumourigenic $CD44^+/CD24^-$ subpopulation with stem cell-like self-renewal properties and the ability to produce differentiated progeny after resveratrol treatment[18]. Compared to vehicle-treated control cells, cells treated with 50 μM resveratrol demonstrated a significant 6-fold decrease in the $CD44^+/CD24^-$ population in MDA-MB-231-luc-D3H2LN cells (Fig. 1b). In addition, mammosphere formation, which has been widely used for breast CSC enrichment, of the $CD44^+/CD24^-$ fraction from MDA-MB-231-luc-D3H2LN cells was suppressed after resveratrol treatment (Supplementary Fig. 1b). We also assessed apoptosis using TUNEL staining and a caspase assay and found that resveratrol did not induce apoptosis (Supplementary Figs. 1c and 1d). Human breast cancers are driven by a CSC component that may contribute to tumour metastasis and therapeutic resistance[20]. Indeed, we found that the combination of resveratrol with low therapeutic doses of docetaxel elicits significantly greater cancer cell growth inhibition *in vitro* and *in vivo* (Supplementary Figs. 1e–g). These findings strongly suggest that resveratrol demonstrates multiple anti-cancer effects through the reduction of the CSC population.

To examine whether resveratrol could influence the breast cancer cell metastasis ability, the highly invasive breast cancer cell line MDA-MB-231-luc-D3H2LN was used in *in vitro* invasion assays. As shown in Fig. 1c, the invasion of MDA-MB-231-luc-D3H2LN cells was suppressed by resveratrol treatment. Previous studies have documented aberrant miRNA expression in cancer, and our observations prompted us to hypothesise that the anti-cancer resveratrol effects were mediated by miRNAs, particularly by a group of tumour-suppressive miRNAs[21]. A recent study has demonstrated that miR-141 and miR-200c strongly inhibit breast cancer invasion ability[22]. We found that resveratrol exposure increases miR-141 and miR-200c expression in MDA-MB-231-luc-D3H2LN cells (Fig. 1d). These findings suggest that resveratrol exhibits multiple anti-cancer effects through the inhibition of CSC phenotypes by activating miR-141 and miR-200c. In addition, to determine whether the up-regulation of miR-141 and miR-200c is mediated at the transcriptional level, we measured the expression levels of the primary miRNAs of miR-141 and miR-200c and found that these miRNAs are up-regulated at the primary transcript level (Supplementary Fig. 1h). Taken together, these results indicate that resveratrol increases the expression of tumour-suppressive miRNAs via the induction of miRNA transcription. Similar results were obtained in two other human breast cancer cell lines (MCF7 and MCF7-ADR) and MCF10A, an immortalised, non-transformed epithelial cell line (Supplementary Figs. 2–4).

Resveratrol up-regulates the expression of tumour-suppressive miRNAs. We demonstrated that resveratrol specifically reduced the CSC fraction (Fig. 1b). In addition, we also observed that miR-141 and miR-200c, which are known to suppress the CSC phenotype, are both induced by resveratrol treatment (Fig. 1d). These observations suggest that a part of the anti-cancer effects of resveratrol is mediated by miRNAs, particularly tumour-suppressive miRNAs. Indeed, a morphological change is observed after resveratrol treatment (Fig. 2a), suggesting that resveratrol induces a variety of miRNAs in cancer cells. To confirm whether miRNAs are globally up-regulated in the multiple anti-cancer effects induced by resveratrol in MDA-MB-231-luc-D3H2LN cells, we performed a comprehensive miRNA profiling of untreated MDA-MB-231-luc-D3H2LN cells and compared the results to those obtained in resveratrol-treated cells. As shown in Fig. 2b, we found that a subset of tumour-suppressive miRNAs is transcriptionally up-regulated by resveratrol (Table 1). To validate the microarray results, we performed qRT-PCR. A set of mature tumour-suppressive miRNAs, including miR-16 and miR-143, are significantly up-regulated in a variety of breast cancer cell lines, including MDA-MB-231-luc-D3H2LN, MCF7, MCF7-ADR, and MCF10A (Supplementary Figs. 2–5). These results indicated that resveratrol globally up-regulates tumour-suppressive miRNAs in human breast normal epithelial and cancer cells.

Resveratrol enhances the Ago2 RNAi potency. Although our data provide evidence that resveratrol globally up-regulates tumour-suppressive miRNAs and one of the mechanisms that is mediated by primary miRNA up-regulation, we also hypothesised that changes at other levels of the RNAi pathway may play a role in enhancing the resveratrol-mediated miRNA activity in cells in addition to transcriptional alterations. It is known that miRNA generation occurs in a multi-step process[23,24]. If one of the components associated with the miRNA pathway is under-expressed or qualitatively impaired, the pathway as a whole is destabilised. To examine the effect of resveratrol on the miRNA machinery, we measured the expression levels of a selected group of miRNA machinery-related genes, including Dicer1, Drosha, TARBP2, DGCR8, and Ago2, after the resveratrol treatment of MDA-MB-231-luc-D3H2LN cells. We found that resveratrol exposure significantly increased Ago2 expression in MDA-MB-231-luc-D3H2LN cells (Fig. 2c and Supplementary Fig. 6a). To elucidate the resveratrol-mediated Ago2 up-regulation mechanism, we assessed the Ago2 promoter activity and the Ago2 mRNA and protein half-lives after resveratrol treatment. As shown in supplementary Fig. 6b, the Ago2 protein half-lives were unchanged after resveratrol treatment. In contrast, the Ago2 mRNA was slightly

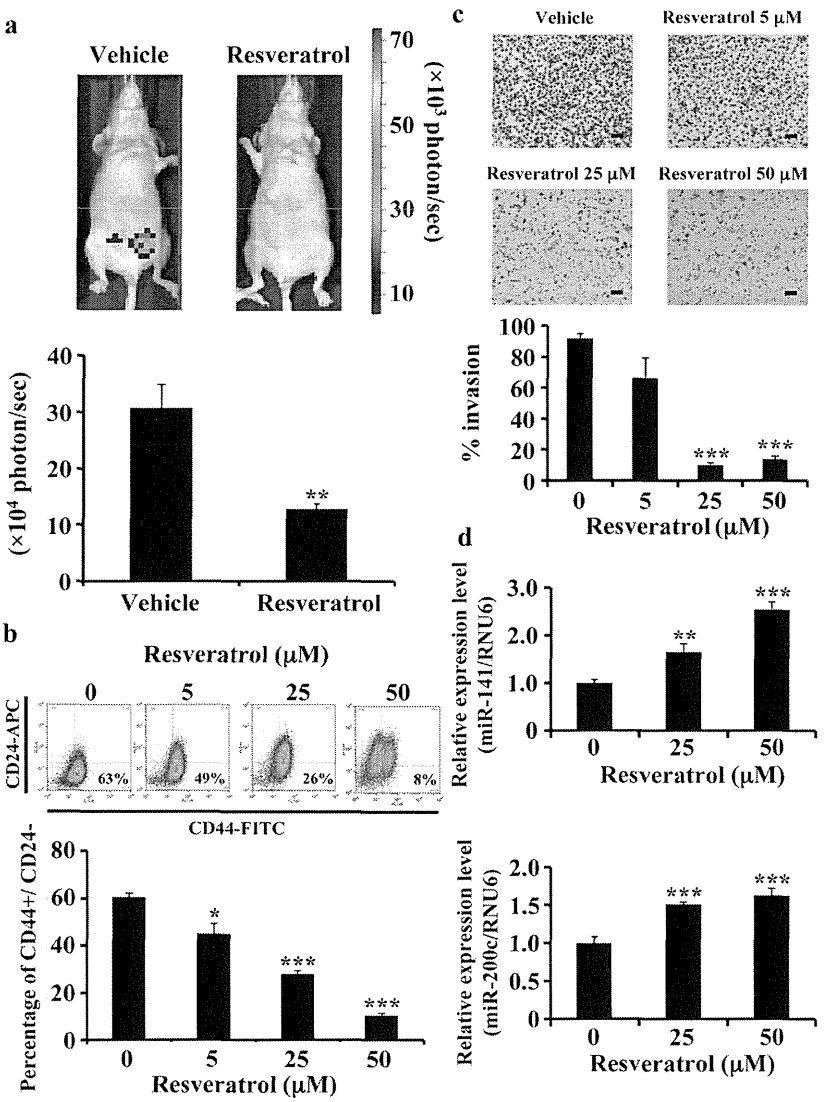

Figure 1 | Multiple anti-cancer effects of resveratrol through the activation of miR-141 and miR-200c. (a) MDA-MB231-luc-D3H2LN cells (200 cells) were injected into the mammary fat pad of six-week-old female SCID hairless outbred mice (n = 5). They were then treated with resveratrol (25 mg/kg/day) by intraperitoneal injection every day for 8 days. Tumour growth was monitored by injecting luciferin in the mice followed by measuring bioluminescence using an IVIS imaging system. Representative mouse images at day 8 (upper panel) and quantified bioluminescence images at day 8 (lower panel) are shown. (b) MDA-MB231-luc-D3H2LN cells were treated with resveratrol or DMSO (control) at the specified doses for 3 days. The percentage of $CD44^+/CD24^-$ cells after compound treatment in independent experiments with MDA-MB231-luc-D3H2LN cell populations is shown. The $CD44^+/CD24^-$ denoting the CSC-enriched fraction. (c) MDA-MB231-luc-D3H2LN cells were grown, treated with resveratrol or DMSO (control) for 1 day, and then subjected to an invasion assay. Representative photographs (upper panel) and quantification (lower panel) are shown. Scale bar: 100 μm. (d) The miR-141 and miR-200c expression levels in MDA-MB231-luc-D3H2LN cells. The expression levels of the indicated miRNAs were examined in MDA-MB231-luc-D3H2LN cells after 48 hour resveratrol treatment (all data are shown as the mean ± s.e.m., *P<0.05, **P<0.01, ***P<0.001).

increased after resveratrol treatment (Supplementary Fig. 6c). In addition, resveratrol induced the luciferase activity of a plasmid containing the Ago2 promoter upstream of the luciferase gene, suggesting that resveratrol transcriptionally induced the expression of Ago2 (Supplementary Fig. 6d). The Ago2 protein is a key regulator of miRNA homeostasis and, upon recognition, it can either cleave or remain tethered to an mRNA to repress its translation and/or regulate its stability[25]. To reveal the relationship between Ago2 and miRNAs, we first quantified the miRNA expression in MDA-MB-231-luc-D3H2LN cells transfected with the Ago2 expression vector. The induction of Ago2 expression by the Ago2 expression vector was confirmed by qRT-PCR (Fig. 2d). After transfection of the Ago2 expression vector, a subset of miRNAs including miR-16, miR-141, miR-143, and miR-200c was higher than in the control cells (Fig. 2e and Supplementary Fig. 6e). To further study the relationship between resveratrol-induced Ago2 and RNAi activity, MDA-MB-231-luc-D3H2LN cells were transfected with luciferase siRNA in the presence of resveratrol treatment and subjected to an *in vitro* firefly luciferase assay. If the induction of Ago2 expression leads to the enhancement of RNAi activity in cells, the luciferase siRNA silencing effect of the luciferase gene in MDA-MB-231-luc-D3H2LN cells may be enhanced after Ago2 over-expression even in the presence of a low siRNA dose and a prolonged period after siRNA transfection. As shown in Fig. 2f, the resveratrol-induced Ago2 resulted in a long-term gene-silencing response in MDA-MB-231-luc-D3H2LN cells. In addition, Ago2 over-expression in HEK293 cells demonstrated a long-term gene-silencing response that was similar to resveratrol-treated MDA-MB-231-luc-D3H2LN cells (Supplementary Fig. 6f).

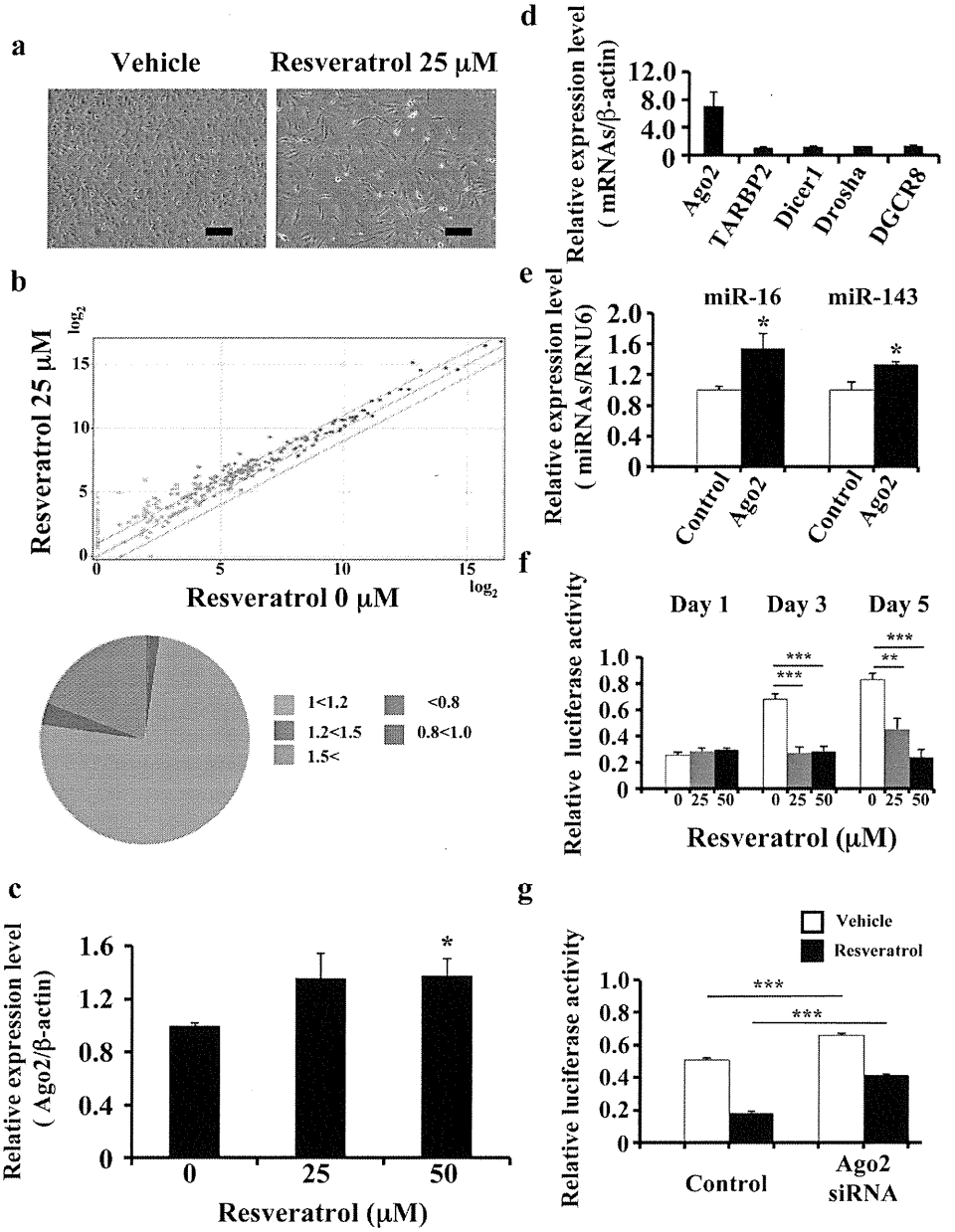

Figure 2 | Association between resveratrol and Ago2. (a) Characteristic microscopic images of MDA-MB231-luc-D3H2LN cells in the presence of DMSO (control) or resveratrol. Scale bar: 100 μm. (b) The effects of resveratrol treatment on miRNA expression in MDA-MB231-luc-D3H2LN cells by miRNA microarray analysis. The proportions of miRNAs at different fold change levels are shown in the lower panel. (c) MDA-MB231-luc-D3H2LN cells were treated with resveratrol or DMSO (control). After 2 days of culture, the cell extract was subjected to real-time mRNA qRT-PCR. (d), (e) MDA-MB231-luc-D3H2LN cells were grown and transiently transfected with Ago2 or EGFP-IRES vector (control). After 2 days of culture, the cell extract was subjected to real-time mRNA (d) and miRNA (e) qRT-PCR. The values on the *y-axis* are depicted relative to the expression level of the EGFP-IRES control vector, which is defined as 1. (f) MDA-MB231-luc-D3H2LN cells were grown and transiently transfected with luciferase siRNA or AllStars negative control siRNA (0.1 nM) under resveratrol treatment. After 1, 3, or 5 days of culture, the cells were subjected to a luciferase reporter assay. The values on the *y-axis* are depicted relative to the luciferase activity of the AllStars Negative Control siRNA, which is defined as 1. (g) MDA-MB231-luc-D3H2LN cells were grown and transiently transfected with luciferase siRNA or AllStars Negative Control siRNA and Ago2 siRNA or AllStars Negative Control siRNA. After 3 days of culture, the cells were subjected to a luciferase reporter assay. The values on the *y-axis* are depicted relative to the luciferase activity of the negative control siRNA, which is defined as 1 (all data are shown as the mean ± s.e.m., *P<0.05, **P<0.01, ***P<0.001).

Moreover, we performed an RNAi experiment to target Ago2 after resveratrol treatment and then assessed the RNAi activity demonstrated by the luciferase siRNA directed against the luciferase gene. The reduction in Ago2 expression by Ago2 siRNA was confirmed by qRT-PCR (Supplementary Fig. 6g). As shown in Fig. 2g, Ago2 siRNA-mediated silencing inhibited the RNAi activity in MDA-MB-231-luc-D3H2LN cells. Taken together, these results indicate that the resveratrol anti-cancer activities were mediated by not only tumour suppressive miRNA upregulation but also by the enhancement of the RNAi activity regulated by Ago2.

Resveratrol-induced miRNA exert an anti-cancer effect. It has been reported that miR-141 inhibits the epithelial-mesenchymal transition and cancer cell migration in breast cancer cells[26]. In addition, we found that resveratrol induced the expression of miR-141 and miR-200c in MDA-MB-231-luc-D3H2LN cells (Fig. 1d). In